The Athena MIMOS II Mössbauer Spectrometer Investigation

G. Klingelhöfer[1], R.V. Morris[2], B. Bernhardt[1], D. Rodionov[1,3], P. A. de Souza Jr.[1,4], S. W. Squyres[5], J. Foh[1], E. Kankeleit[6], U. Bonnes[6], R. Gellert[1], Ch. Schröder [1], S. Linkin[3], E. Evlanov[3], B. Zubkov[3], and O. Prilutski[3]

[1]Institut Inorg. & Analytical Chemistry, Johannes Gutenberg-University, 55099 Mainz, Germany

[2]NASA Johnson Space Center, Houston, TX 77058, USA

[3]Space Research Institut IKI, Moscow, Russia

[4]Pelletizing Department, Companhia Vale do Rio Doce, Vitoria, ES, Brazil

[5]Cornell University, Ithaca, NY 14853,USA

[6]Nuclear Physics Institut, Darmstadt University of Technology, 64289 Darmstadt, Germany

Submitted to *J. Geophys. Res.*

Special issue on the Mars Exploration Rover mission

Correspondence Address:

Goestar Klingelhoefer
Johannes Gutenberg-Universitaet Mainz
Fachbereich Chemie und Pharmazie
Institut fuer Anorganische und Analytische Chemie
Staudinger Weg 9
D-55099, Mainz, Germany
Phone: +49-6131-392-3282
Email: klingel@mail.uni-mainz.de

Abstract. Mössbauer spectroscopy is a powerful tool for quantitative mineralogical analysis of Fe-bearing materials. The miniature Mössbauer spectrometer MIMOS II is a component of the Athena science payload to be launched to Mars in 2003 on both Mars Exploration Rover missions. The instrument has two major components: (1) a rover-based electronics board which contains power supplies, a dedicated central processing unit, memory, and associated support electronics and (2) a sensor head that is mounted at the end of the instrument deployment device (IDD) for placement of the instrument in physical contact with soil and rock. The velocity transducer operates at a nominal frequency of ~25 Hz and is configured with two ^{57}Co/Rh Mössbauer sources. One source (~5 mCi landed intensity), together with a reference target (α-Fe_2O_3 plus α-Fe^0) and PIN diode detector in transmission geometry, are internal to the sensor head and is used for instrument calibration. The other source (~150 mCi landed intensity), together with four PIN diodes in backscatter measurement geometry, irradiates Martian surface materials with a beam diameter of ~1.4 cm after passing through a collimator. Physical contact with surface materials is sensed with a switch-activated contact plate. The contact plate and internal reference target are instrumented with temperature sensors. Assuming ~18% Fe for Martian surface materials, experiment time is 6-12 hours during the night for quality spectra (i.e., good counting statistics); 1-2 hours is sufficient to identify and quantify the most abundant Fe-bearing phases. Data stored internal to the instrument for selectable return to Earth include Mössbauer and pulse-height analysis spectra (256 channels each) for each of the five detectors in up to 13 temperature intervals (65 Mössbauer spectra), engineering data for the velocity transducer, and temperature measurements. The total data volume is ~150 kByte. The mass and power consumption are ~500 g (~400g for the sensor head) and ~2 W, respectively.

The scientific measurement objectives of the Mössbauer investigation are to obtain for rock, soil, and dust (1) the mineralogical identification of iron-bearing phases (e.g., oxides, silicates, sulfides, sulfates, and carbonates), (2) the quantitative measurement of the distribution of iron among these iron-bearing phases (e.g., the relative proportions of iron in olivine, pyroxenes, ilmenite and magnetite in a basalt), and (3) the quantitative measurement of the distribution of iron among its oxidation states (e.g., Fe^{2+}, Fe^{3+}, and Fe^{6+}). Special geologic targets of the Mössbauer investigation are dust collected by the Athena magnets and exterior and interior rock and soil surfaces exposed by the Athena Rock Abrasion Tool and by trenching with rover wheels, respectively.

1. Introduction

Iron Mössbauer spectroscopy (FeMS) has been used in Earth-based laboratories to study the mineralogical composition of iron-bearing phases in a variety of planetary samples, including lunar samples returned to Earth by American Apollo astronauts and Soviet robotic missions and meteorites that have asteroidal and Martian origins [e.g., *Fernandez et al*., 1970; *Gay et al*., 1970; *Herzenberg and Riley*, 1970; *Herzenberg et al*., 1971; *Housley et al.,* 1970, 1971, 1973; *Huffman et al.*, 1974; *Wdowiak and Agresti*, 1984; *Madsen et al*., 1986; *Vieira et al.,* 1986; *Solberg and Burns*, 1989; *Burns and Martinez*, 1991; *Burns*, 1993; *Morris et al.*, 1998; *Graff et al.*, 2003]. A variety of terrestrial samples that are analogues of Martian surface regions have also been studied by FeMS [e.g., *Morris et al.*, 1989, 1990, 1993, 1995, 1996, 1997, 1998, 2000, 2001a; *Burns and Fisher*, 1990; *Straub et al.*, 1991; *Bell et al.*, 1993; *Fegley et al.*, 1995; *Golden et al*., 1993; *Bishop et al.*, 1993, 1995; *Bishop and Murad*, 1996; *Klingelhöfer et al.*, 1996; *Wade et al.*, 1999; *Lane et al.*, 2002]. To date, no in situ FeMS measurements have been made as part of any planetary mission. With the launch in 2003 of Mössbauer spectrometers aboard the European Space Agency (ESA) Beagle-2 mission and the two Mars Exploration Rover (MER) missions, this situation is about to change.

The scientific basis for landing a Mössbauer spectrometer on Mars is extensively discussed by Knudsen [*Knudsen,* 1989; *Knudsen et al.*, 1990, 1992]. The scientific objectives of the MIMOS II Mössbauer spectrometer investigation are (1) to identify the mineralogical composition and (2) to measure the relative abundance of iron-bearing phases (e.g., silicates, oxides, carbonates, phyllosilicates, hydroxyoxides, phosphates, sulfides, and sulfates), (3) to distinguish between magnetically ordered and paramagnetic phases and provide, from measurements at different temperatures, information on the size distribution of magnetic particles, and (4) to measure the distribution of Fe among its oxidation states (e.g., Fe^{2+}, Fe^{3+}, and Fe^{6+}). These data characterize the present state of Martian surface materials and provide constraints on climate history and weathering processes by which the surface evolved to its present state. FeMS can, for example, identify primary igneous minerals such as iron-bearing olivine and pyroxene and weathering products which do (e.g., goethite and jarosite) and do not (e.g., hematite and maghemite) contain volatiles as a part of their structures. Iron-bearing sulfides (e.g., pyrite and phyrrhotite) and carbonates (e.g., siderite) can also be detected.

By determining the size distribution of iron oxide particles, Mössbauer analyses can differentiate between, for example, low-temperature (e.g., nanophase ferric oxide particles) formed during palagonitization [e.g., *Morris et al.*, 2000, 2001a]) and hydrothermal (e.g., hematite particle formation during associated with an impact event into a water-rich target [e.g., *Morris et al.*, 1996]) alteration processes. Another question is whether the Martian meteorites can be related to actual materials on the Martian surface. Mössbauer spectroscopy can directly address this question through comparison of laboratory Mössbauer spectra for Martian meteorites and in situ spectra for the Martian surface.

This paper is divided into five main sections. In Section 2, we briefly discuss the principles of Mössbauer spectroscopy. In Section 3, we give a technical description the MIMOS II Mössbauer spectrometers that were fabricated for the two MER rovers and the Mars –Express Beagle-2 lander. MIMOS II performance validation on geologic samples is discussed in Section 4. In Section 5, we develop operational considerations, including analysis of Mössbauer spectra returned from Mars.

2. Principles and Practice of Mössbauer Spectroscopy

2.1 The Mössbauer Effect for ^{57}Fe

The Mössbauer effect, the recoilless emission and resonant absorption of γ-rays by certain nuclei in solid materials (in our application, ^{57}Fe), has been extensively reviewed in the literature [e.g., *Wertheim*, 1964; *Greenwood and Gibb*, 1971; *Bancroft,* 1973; *Hawthorne,* 1988; *Burns and Solberg*, 1990; *Burns*, 1993]. We give a brief overview here from the perspective of application to Martian surface materials.

Resonant absorption and emission of γ-rays means that absorbed and emitted γ-rays have precisely the same energy. The requirement for this to occur with non-zero probability is that the absorbing and emitting nuclei must be in solid lattices having sufficient mass so that there is no nuclear recoil energy (i.e., "recoilless" nuclear transitions). Because kinetic energy ($=p^2/2m$, where p and m are momentum and mass, respectively) is inversely proportional to mass at constant momentum, the recoil energy is virtually zero when the mass of the solid lattice is $\sim 10^{18}$ times the nuclear mass, i.e., a small particle weighing ~0.1 mg. Even in a solid, however, the emission (or absorption) of the γ-rays can involve energy transfer to lattice vibrations (phonons) in the crystal so that the Mössbauer effect is not observed. The probability of emissions that take

place without inducing any phonons is named, as in X-ray diffraction, the Debye-Waller factor f_D. In general, this factor depends on temperature, the Debye temperature of the crystal, and the γ-ray energy [*Gonser, 1986*]. The probability of recoilless emission or absorption is 0.76 for ^{57}Fe in α-Fe^0 at room temperature.

The energies of γ-rays from recoilless emissions are very precise (14.401 keV for ^{57}Fe), and their energy distribution has a Lorentzian line shape with a width of ~4.7 neV that approaches the theoretical width imposed by the Heisenberg uncertainty principle. This width is in general less than the difference in energy between nuclear energy levels that result from different nuclear environments caused by, for example, different oxidation states and/or mineralogical environments. Therefore, recoilless emission of 14.4 keV γ-rays by ^{57}Fe in one lattice will not undergo recoilless absorption in another lattice if the nuclear environments are too different, unless the energy of the emitted γ-ray or the energy of the nuclear energy levels in the absorber is changed slightly. Usually, the energy of emitted recoilless γ-rays is changed using the Doppler effect, i.e., by moving the source. For ^{57}Fe, energy "scanning" through limits of ±10 mm/s is sufficient. The Mössbauer spectrum is then counts passing through (or emitted by) an absorbing sample as a function of the relative velocity of the source and sample.

The nuclear energy levels of ^{57}Fe (ground and first excited states with nuclear spins of 1/2 and 3/2, respectively) can be changed by electric or magnetic fields acting at the nucleus. The processes, called hyperfine interactions, are the electrical monopole interaction, the electrical quadrupole interaction, and the nuclear Zeeman interaction. The hyperfine interactions can be translated into three parameters that are measured from Mössbauer spectra by curve fitting, and it is these parameters that characterize the oxidation state and mineralogical environment of the ^{57}Fe nucleus, which has ~2.2% natural abundance. We discuss these derived parameters next. The energy level diagrams are shown schematically in Figure 1.

2.1.1 The isomer shift (IS, mm/s). The electrical monopole interaction is the interaction of the nuclear charge with the electron density at the nucleus. This interaction occurs primarily with *s* electrons, because they have non-zero probability of being located at the nucleus. If nuclear energy levels of ^{57}Fe in both the source and absorber are not split, the difference in energy (velocity) between the source and absorber is the isomer shift (IS). Normally, ^{57}Co, which decays to first excited state of ^{57}Fe and subsequently undergoes recoilless emission of the 14.4 keV Mössbauer γ-ray with high probability by decay to the ground state, is used as the emission

source for Fe Mössbauer spectroscopy. When imbedded in a matrix that has high symmetry (normally Rh metal), monochromatic γ-rays are emitted because the ^{57}Fe nuclear states are not split. The usual practice is to report the values of IS relative to the midpoint of the Mössbauer spectrum for α-Fe^0

2.1.2 The quadrupole splitting (QS, mm/s). When the site symmetry at the ^{57}Fe nucleus is below cubic, an electric field gradient may be present there. This gradient interacts with the nuclear quadrupole moment and splits the energy level of the excited state into two states (±1/2 and ±3/2), so that two transitions (a doublet) are possible (Figure 1). The magnitude of the quadrupole splitting is the absolute value of the difference in velocity of the two lines of the doublet. When the angle between the direction of propagation of the incident γ-rays and the direction of the electric field gradient is randomly distributed (as in a polycrystalline sample), the doublet lines have equal intensity. The intensity ratios are 3:1 and 5:3 when the angle equals 0º and 90º, respectively.

2.1.3 The internal magnetic field (B_{hf}, T). When a magnetic field is present at the nucleus, all of the nuclear energy levels are split (nuclear Zeeman effect), and six transitions are possible under the constraint of spin allowed transitions (nuclear spin changes of 0 and ±1 as in Figure 1). The magnetic field can be an intrinsic property of the material or can imposed by an external magnet. When there is no electric field gradient present (QS=0), the six lines are symmetrically placed about the midpoint of the spectrum. This is the case for α-Fe^0. The magnitude of the internal field can be calculated from the absolute value of the difference position of the lines at highest and lowest velocity (B_{hf} = |(6-1)|).

The situation when both an electric field gradient and an internal magnetic field are present can be very complicated. Fortunately, in most cases the magnetic interaction is much stronger, and the electrical interaction can be treated as a perturbation. In this case, QS can be calculated from the formula QS = ½[(6-5)-(1-2)], where the numbers refer to the lines of the sextet numbered from lowest to highest velocity. B_{hf} is calculated as described above.

The relative intensities of the lines in the sextet depend on the angle between the propagation direction of the incident γ-rays and the direction of magnetization. When the directions are randomly distributed (isotropic) as is often the case for a powder, the intensity ratios are 3:2:1:1:2:3. When the angle is 90°, the intensity ratio is 3:4:1:1:4:3. When the angle is 0°, the intensity ratio is 3:0:1:1:0:3, i.e., lines 2 and 5 are not present.

2.2 Basic Mössbauer Instrument Design

Standard laboratory Mössbauer spectrometers have a velocity transducer, wave form generator and synchronizer, multichannel analyzer, γ-ray detection system, a velocity calibration device, a radiation source (normally ^{57}Co in a Rh metal matrix for ^{57}Fe Mössbauer spectroscopy), computer, and optionally a cryostat or oven for temperature-dependent measurements. In transmission measurement geometry (Figure 2), the absorber (sample) is between the source and detector, so that negative peaks are observed corresponding to absorption of 14.4 keV γ-rays. In backscatter (or emission) measurement geometry, the source and detector are on the same side of the emitter (sample), so that positive peaks are observed corresponding to emission of 14.4 keV γ-rays. In backscatter geometry, emitted internal conversion X-rays or electrons can also be detected to produce Mössbauer spectra.

Mössbauer spectra are generated by the velocity-sweep method in which the velocity transducer moves the source (or sample) repeatedly over a range of velocities, while simultaneously γ-rays transmitted through (or emitted by) the sample are counted into synchronized channels. In most instruments, the source is mounted on the vibration axis of an electromagnetic transducer (loudspeaker system) which is moved according to a voltage waveform applied to the driving coil of the system. Typically, the transducer is operated at constant acceleration with a triangular waveform at a frequency of 10-50 Hz. Detector counts are stored in a memory (typically 1024 channels). Synchronization of the channel number in the memory and the instantaneous velocity of the source is achieved by advancing the memory address one by one. This is done through an external clock which subdivides the period of the waveform applied to the drive system into the number of available channels. The triangular waveform and 1024 memory channels produces two mirror-imaged Mössbauer spectra each with 512 channels. They can be combined (to increase the signal to noise ratio) to give one 512 channel Mössbauer spectrum.

2.3 Basics of Mössbauer Data Analysis

In the simplest case for transmission measurements on an ideal absorber, Mössbauer spectra are the superposition of one or more peaks with Lorentzian lineshapes whose areas are proportional to the number of absorbing nuclei times the recoiless fraction *f*. An ideal absorber

has ~10 mg/cm^2 of natural Fe and is uniform. Uniformity is achieved by using sufficiently fine powders. The relative abundance of Fe associated with specific Fe-bearing phases is therefore equal to the sum of the *f*-factor-normalized relative peak areas all peaks associated with that phase. Mössbauer spectra are deconvolved into component peaks using computer programs to perform linear-least square fits where the lineshape function (e.g., Lorentzian and Voigt) is a selectable parameter. From peak positions calculated from the least-square fit, values of Mössbauer parameters IS, QS, and B_{hf} can be calculated and phase identifications made or constrained. Relative proportions of Fe associated with the specific Fe-bearing phases are calculated from peak areas and relative *f*-factors. Large compilations of Mössbauer parameters for geologically-relevant materials are publically available [e.g., *Burns and Solberg*, 1990; *McCammon,* 1995; *Stevens et al.*, 1998]. *De Grave and Van Alboom* [1991] report *f*-factors for Fe^{2+} and Fe^{3+} for a number of geologically relevant minerals.

2.4 Special considerations for MER and Beagle-2

2.4.1 Backscatter measurement geometry. Because of the complexity of sample preparation, backscatter measurement geometry is the choice for an in situ planetary Mössbauer instrument [e.g., *Morris et al.*, 1988; *Galazkha-Friedman*, 1989]. No sample preparation is required, because the instrument is simply presented to the sample for analysis. On MER, the MIMOS II sensor head is mounted on a robotic arm that places it in physical contact with the analysis target (e.g., rock or soil) [*Squyres et al*., this issue]. MIMOS II is similarly mounted on Beagle-2 [*Sims et al*, 2002].

As discussed above, successful acquisition of Mössbauer spectra depends on accurate knowledge of the relative velocity of the source and sample. External vibrations that impart differential velocity components to the source and sample would degrade the quality of the Mössbauer spectrum. This degradation ranges from slight line broadening in mild cases to complete obliteration of the Mössbauer spectrum in severe cases. External vibrations are not generally a problem in laboratory settings because the sample and velocity transducer are rigidly held. On Mars, wind-induced vibrations are an obvious environmental factor that might degrade the quality of Mössbauer spectra. However, backscatter spectra obtained for hematite with a prototype MIMOS II instrument during field tests did not show detectable line broadening [*Arvidson et al.*, 1998]. The MER Instrument Deployment Device (IDD) has been designed to

assure that velocity noise at the MIMOS II sensor head will not exceed 0.1 mm/sec [*Squyres et al*., this issue].

2.4.2 Sampling depth. In addition to no requirement for sample preparation, backscatter measurement geometry has another important advantage. Emission of internal conversion electrons, Auger electrons, and X-rays, which occur along with the recoilless emission and absorption of the 14.4 keV γ-ray of ^{57}Fe, can also be used for Mössbauer measurements. For ^{57}Fe, internal conversion X-rays have an energy of 6.4 keV. Because the penetration depth of radiation is inversely proportional to energy, the average depth from which 14.4 keV γ-rays emerge in emission measurements is greater than that for 6.4 keV X-rays. The importance of this difference in emission depths for an in situ Mössbauer spectrometer is that mineralogical variations that occur over the scale depths of the 14.4 and 6.4 keV radiations can be detected and characterized. Such a situation on Mars might arise for thin alteration rinds and dust coatings on the surfaces of otherwise unaltered rocks.

Sampling depths can be estimated by calculation and by laboratory measurements. Figure 3 [after *Morris et al.*, 2000] shows by direct calculation that the sampling depth is ~50-200 μm for solid basaltic rock and ~500-2000 μm for fine grained basaltic dust for 15 keV γ-rays (i.e., approximately the same energy as the 14.4 keV ^{57}Fe γ-ray). These calculations were confirmed by *Morris et al.* [2001b] who performed backscatter Mössbauer measurements of basaltic dust deposited to various thicknesses on rock substrates. These results show that we can "see" through a significant layer of dust coating and obtain mineralogical information about the underlying rock. In Figure 4, an example is given for a sandwich structure composed of foils of α-Fe^0, aluminum, and stainless steel. The 6.4 keV X-rays are detected from only the shallower α-Fe^0 foil, and the 14.4 γ-rays are detected from both the α-Fe^0 and SS foils.

2.4.3 Cosine smearing. Because instrument volume and experiment time must both be minimized for a planetary Mössbauer spectrometer, it is desirable in backscatter geometry to illuminate as much of the sample as possible with source radiation. However, this requirement at some point compromises the quality of the Mössbauer spectrum because of an effect known as "cosine smearing". The energy of the 14.4 γ-rays incident on the sample is a function both the velocity of the source and angle (θ) between the axis of source motion and the emission angle of source γ-rays. The energy is changed by a factor of cosθ, which gives the effect its name. The effect of cosine smearing on the Mössbauer spectrum is to increase the linewidth of Mössbauer

peaks (lowers resolution) and shift their centers outward (affects values of Mössbauer parameters). Therefore, the diameter of the source "γ-ray beam" incident on the sample, which is determined by a collimator, is a compromise between acceptable experiment time and acceptable velocity resolution. For coaxial symmetry, *Aramu and Maxia* [1970] calculated that when the ratio of the collimator radius and the distance between the source and the collimator is ≤0.1, cosine smearing can be neglected. Note that the distortion in peak shape resulting from cosine smearing can be accounted for mathematically in spectral fitting routines, but the reduction in resolution can lead to irretrievable loss of information. *Riesenman et al*. [1969] derived a formula for the peak shape when cosine smearing is present for coaxial symmetry in transmission measurement geometry. Geometrical considerations are more complicated for MIMOS II, where backscatter measurement geometry is employed and the symmetry, although coaxial for the excitation process, is more complex for detection. *Held* [1997] solved this problem mathematically, and implemented the result in the fitting routines we use.

2.4.4 Orientation effects. Because Martian surface material will be analyzed by Mössbauer spectrometers without sample preparation, variations in line intensity resulting from orientation effects are a strong possibility. This is especially the case for rocks with coarse grained mineral constituents, for example single-crystal phenocrysts of olivine whose dimensions are comparable to the Mössbauer source "beam diameter" (~14 mm) that is incident on the sample. Orientation effects may also be present in Martian soil. For example, thermal emission spectra of the Meridiani Planum region that were obtained from Martian orbit by the Mars Global Surveyor Thermal Emission Spectrometer instrument have been interpreted in terms of an orientation effect for platy hematite crystals [*Christensen et al.*, 2000, 2001; *Lane et al.*, 2002]. This orientation effect would also be detected by Mössbauer spectroscopy [*Gonser et al*., 1991]. Meridiani Planum is one of the landing sites for the MER rovers.

Orientation effects and/or induced hyperfine splitting (or spectral broadening) are also important considerations for Mössbauer spectra acquired on material collected on the permanent magnets mounted on MER rover decks [*Madsen et al.*, this issue].

2.4.5 Temperature variation. Mössbauer parameters for many materials vary strongly with temperature. For laboratory instruments, sample temperature can be changed and held at different temperatures by ovens and cryostats for as long as necessary for determination of Mössbauer parameters as a function of temperature. During a typical overnight Mössbauer

experiment on Mars, however, the sample temperature will vary by many tens of degrees. To both ensure the quality of Martian Mössbauer spectra (i.e., prevent line broadening from temperature dependent Mössbauer parameters) and to measure of any temperature dependence in Mössbauer parameters (which aids in phase identification), a Mössbauer spectrometer on Mars must be able acquire and separately store spectra as a function of temperature.

3. MIMOS II Instrument Description

3.1 Design overview

Because of mission constrains for minimum mass, volume, and power consumption, the MIMOS II is extremely miniaturized compared to standard laboratory Mössbauer spectrometers and is optimized for low power consumption and high detection efficiency [*Klingelhöfer et al.*, 1998, 1999]. All components were selected to withstand high acceleration forces and shocks, temperature variations over the Martian diurnal cycle, and cosmic ray irradiation. Because of restrictions in data transfer rates, most instrument functions and data processing capabilities, including acquisition and separate storage of spectra as a function of temperature, are performed by an internal dedicated microprocessor (CPU) and memory. The dedicated CPU is also required because most Mössbauer measurements will be done at night when the rover CPU is turned off to conserve power. High detection efficiency is extremely important in order to minimize experiment time. Experiment time is also minimized by using as strong a main ^{57}Co/Rh source as possible. Because the half life of ^{57}Co (271 days) is not much longer than the 6-7 month duration of the journey to Mars, this implies a design and schedule that allows the source to be manufactured, delivered, and mounted in MIMOS II as close to launch as possible. Instrument internal calibration is accomplished by a second, less intense radioactive source mounted on the end of the velocity transducer opposite to the main source and in transmission measurement geometry with a reference sample. For MER, the spectrometer can also be calibrated with the magnetite Compositional Calibration Target (CCT) which is mounted on the rover body [*Squyres et al*., this issue.].

Physically, the MIMOS II Mössbauer spectrometer has two components that are joined by an interconnect cable: the sensor head and electronics printed-circuit board. On MER, the sensor head is located at the end of the IDD and the electronics board is located in an electronics box inside the rover body. On Mars-Express Beagle-2 the sensor head is mounted also on a

robotic arm integrated to the PAW instrument assembly. The sensor head (Figures 5 and 6) contains the electromechanical transducer (mounted in the center), the main and reference ^{57}Co/Rh sources, multilayered radiation shields, detectors and their preamplifiers and main (linear) amplifiers, and a contact plate and sensor. The contact plate and sensor are used in conjunction with the IDD to apply a small preload when it places the sensor head, holding it firmly against the target. The electronics board contains power supplies/conditioners, the dedicated CPU (a 8051 type microprocessor), different kinds of memory, firmware, and associated circuitry for instrument control an data processing.

3.2 Mössbauer sources, shielding, and collimator

The highest possible source activity is desirable, with the constraint that the source line width should not increase significantly (maximum by a factor of 2-3) over the ~9-12 months duration of the mission. Calculations and tests indicate an optimum specific activity for ^{57}Co at 1 Ci/cm^2 [*Gummer,* 1988; *Evlanov et al.,* 1993]. Sources of ~330 mCi ^{57}Co/Rh with a specific activity close to this value and extremely narrow source line width (<0.13 mm/s at room temperature) given the high activity, were produced by Cyclotron Co. Ltd. (Russia) in custom made space-qualified Ti-holders, tested successfully, and mounted in flight instruments approximately 90 days prior to launch. No additional line broadening will result at lower temperatures on Mars with the rhodium matrix.

Very important is an effective shielding of the detector system from direct and cascade radiation from the ^{57}Co/Rh source. A graded shield consisting of concentric tubes of brass, tantalum, and lead was selected. The thickness and the shape of different parts of the shielding were optimized so that nearly no direct 122 keV radiation (emitted by the ^{57}Co) is in a direct line with the detectors.

The shielding also acts as the collimator which fixes the diameter of the target that is illuminated by γ-rays. As discussed previously, this diameter is as large as possible to minimize experiment time within the constraint of acceptable cosine smearing [*Klingelhoefer et al*., 1992]. The measure used for acceptable cosine smearing was the ability to reliably resolve the strongly overlapping spectra of hematite and maghemite in a 1:1 mixture of those oxides. A series of experiments with this mixture and the pure oxides were conducted at constant source intensity and variable collimator radius between 2.25 and 3.55 mm, which corresponds to an illumination

diameter of ~12 and ~17 mm, respectively [*Schröder*, 2001]. The spectra were analyzed using the fitting routine developed by *Held* [1997]. Analysis of the mixture spectra reproduced the Mössbauer parameters for and relative proportions of the individual oxide components for collimator diameters of 4.50 and 5.60 mm. For collimator diameters of 6.20 and 7.10 mm, the calculated and actual relative proportions of the oxides differ significantly. Therefore, a collimator diameter of 5.60 mm was selected for MIMOS II flight instruments. This diameter limits the maximum γ-ray emission angle to ~25° and gives a "beam diameter" of ~14 mm on the sample. As expected, because cosine smearing was observed, the ratio of collimator radius to source-collimator distance (0.25) is considerably larger than the <0.1 value required for the effect to be negligible.

3.3 Drive system

The simplest way to meet volume and weight constraints was to scale down drive systems we have built for laboratory instruments for many years [*Kankeleit,* 1964, 1975]. We constructed a drive system which had about one fifth the size of a standard laboratory system. It has a diameter of 22 mm, a length of 40 mm, and ~50 g mass [*Teucher*, 1994].

The MIMOS II design is based on a rigid tube connection between drive and the velocity pick-up coils in the double-loudspeaker arrangement with good electrical and magnetic shielding between the two coils to avoid crosstalk. The intense main ^{57}Co/Rh source is mounted at one end of the tube, and the weaker source for the reference absorber is mounted at the other end. The short tube guarantees a fast transfer of information with the velocity of sound in the aluminum and thus a minimum phase lag and a high feedback gain margin. Fortunately, and despite the increase of unwanted crosstalk resulting from the smaller distance between the coils, the crosstalk relative contribution is still less than 0.01% in the frequency domain of the triangular waveform and is therefore negligible. The system is equipped with SmCo permanent magnets and was optimized to give a homogeneous and high magnetic field in the coil gaps. To do this, the specialized computer program PE2D, designed to calculate magnet systems for charged particle storage rings in high energy physics, was used for calculation and optimization of the drive magnet system. We found good correspondence between calculated and experimental magnetic field measurements that were performed using a Hall sensor [*Teucher*, 1994].

The drive operates at a frequency of ~25 Hz, which is also its main resonance (Figure 7). This low frequency allows a broad bandwidth for the closed loop system, and good performance with a triangular reference signal, but requires rather soft Kapton springs. As a consequence, rotation of the drive from horizontal to vertical position in Earth gravity leads to a shift of about 0.4 mm from the equilibrium position of the tube. However, the resulting non-linearity between velocity and pickup voltage remains <0.1% at room temperature. Although this shift could be compensated by a DC current, no correction is needed for a mission to Mars where the gravity forces are smaller by a factor of ~3. In order for the drive to operate over expected Martian surface temperatures (80 – 283 K), it was necessary to degrade the linearity to ~3%.

The design provides limiters to avoid destruction of the Kapton springs during the large accelerations associated with launch and landing. Vibration and shock tests of the drive system with levels up to, and slightly exceeding the specifications for both MER and Beagle-2 missions were successfully performed.

3.4 Detector system and electronics

The main disadvantage of the backscatter measurement geometry employed by MIMOS II is the secondary radiation caused by primary 122 keV radiation from the decay of ^{57}Co. To reduce the background at the energies of the14.4 keV γ-ray and the 6.4 keV X-ray lines, a detector with good energy resolution is required. In addition, an intense main ^{57}Co source and a detector system covering a large solid angle are needed to minimize data acquisition time. Good resolution is even more important should it prove possible to use these detectors for elemental analysis with the X-ray fluorescence technique (i.e., using the pulse height analysis (PHA) spectra that are also acquired as a part of our measurement procedure). For this reason, four Si-PIN-diodes with a 10 x 10 mm^2 active area were selected as detectors [*Weinheimer et al.,* 1992; *Held,* 1993a,b] instead of gas-counters as considered by other authors [*Prilutskii*, 1990; *Agresti et al.,* 1992]. A detector thickness of about 400-500 μm is a good choice according to our calculations and experience. The energy resolution is ~1.0-1.5 keV at room temperture, and it improves at lower temperaures. The efficiencies at 6.4 and 14.4 keV are nearly 100 % and about 70 %, respectively [*Held*, 1993a,b].

The 100 V DC bias voltage for the detector diodes is generated by high frequency cascade circuitry with a power consumption of less than 5 mW. Noise contributions are minimized by incorporating a preamplifier-amplifier-SCA system for each individual detector.

Spectra of ^{57}Co/Rh radiation backscattered from an aluminum (Al) and a stainless steel (SS) plate (same recording times) are shown in Figure 8. A continuum is seen above 122 keV resulting from the few 692 keV γ-rays which are not completely absorbed in the shielding. Although no photo peak appears at 122 keV, this radiation shows up as a broad Compton distribution being more intense for the lower Z aluminum. A second Compton distribution originates in the detector itself as seen in the rising slope starting below 40 keV. The peak at 22.1 keV results from the silver (Ag) backing of the detector. Below this energy the 14.4 keV Mössbauer resonance line and also the 6.4 keV X-ray line dominate in SS at zero velocity, in contrast to Al where only the (14.4 - 0.4) keV Compton scattered line appears.

In addition to the four detectors used to detect backscattered radiation from the sample, there is a fifth detector to measure the transmission spectrum of the reference absorber (α-^{57}Fe plus α-$^{57}Fe_2O_3$ Sample and reference spectra are recorded simultaneously, and the known temperature dependence of the Mössbauer parameters of the reference absorber can be used to give a measurement of the average temperature inside the sensor head, providing a redundancy to measurements made with the internal temperature sensor.

3.5 Temperature measurement

MIMOS II has three temperature sensors: one on the electronics board in the Rover warm electronics box and two on the sensor head (Analogue Devices AD590). One temperature sensor in the sensor head is mounted near the internal reference absorber, and the measured temperature is associated with the reference absorber and the internal volume of the sensor head. The other sensor is mounted outside the sensor head at the contact ring assembly. It gives the approximate analysis temperature for the sample on the Martian surface. This temperature is used to route the Mössbauer data to the different temperature intervals (maximum of 13, with the temperature width software selectable) assigned in memory areas. An example of a simulated overnight experiment on Mars is shown in Figure 9 for eight temperature intervals using the CCT as the target. The eight backscatter spectra collected from the target and the corresponding eight

velocity reference spectra are in Figure 9a and Figure 9b, respectively. In case of contact-ring temperature sensor failure, the internal temperature sensor would be used (software selectable).

During measurements, a temperature log is acquired for all three sensors. Temperature measurements are done approximately every 5 min (software selectable: min ~10 sec, max ~40min). MIMOS II can accumulate up to 256 temperature records corresponding to a total integration time of ~21 hours.

3.6 Operation modes and software

3.6.1 MIMOS II operational modes. The instrument can be operated in six different modes depending on the nature of the requirement. (1) Mössbauer temperature-dependent mode. Mössbauer sample and reference spectra are collected and stored as a function of up to 13 temperature intervals. The temperature ranges are variable and can be changed during mission operations. (2) Mössbauer temperature independent mode. Mössbauer and reference spectra are collected irrespective of the sample or reference temperature. (3) Energy mode. PHA spectra are collected to determine detector performance and to make changes in energy-window settings. (4) Engineering mode. The drive differential signal is collected to determine the velocity drive performance. (5) Idle mode. In this mode, no operations are performed. (6) Standard mode. This mode is used for normal operations. It consists of the Engineering, Energy, and Mössbauer temperature dependent modes commanded sequentially.

3.6.2 Data structure, temperature log, and backup strategy. One Mössbauer spectrum consists of 512 velocity channels (3 bytes/channel). One temperature interval consists of five Mössbauer spectra (one for each detector). There are 13 temperature intervals with selectable width. Thus, MIMOS II can accumulate up to 65 Mössbauer spectra during one experiment session on Mars. All Mössbauer, energy, engineering and temperature data taken during this session are stored in a volatile SRAM memory (128 KB) on the MIMOS II electronics board.

Firmware parameters and the instrument logbook are stored in the non-volatile memory ferroelectric RAM (FRAM) on the electronics board. There are three individual FRAMs on the MIMOS II electronics board with three identical copies of these parameters to ensure parameter integrity. The copies are verified and compared to each other from time to time to verify they are identical. If one copy deviates from the other two, it will be replaced by a copy of the two other still identical parameter sets. All parameters can be adjusted during mission operations.

To minimize risk of data loss because of power failure or other reasons, the Mössbauer data are copied to a non-volatile EEPROM memory every 9 minutes (software selectable). As the size of the EEPROM is smaller than the SRAM, the EEPROM can accumulate only up to ten Mössbauer spectra as a subset of the data from the SRAM. These spectra are obtained from the SRAM according to a pre-defined summation strategy.

3.7 Velocity and energy calibration

3.7.1 Velocity calibration. The interpretation of acquired Mössbauer spectra is impossible without knowing the drive velocity precisely at any given time. Mössbauer drive velocity calibration for MIMOS II is rather straightforward and done in three different ways, thus ensuring redundancy. Prior to flight each individual drive system was calibrated by measuring in backscattering mode an α-iron foil standard. A maximum drive velocity was preset by firmware. Fitting the acquired Mössbauer spectrum using the well known parameters of the α-iron foil then yielded the real velocity. The results for a MIMOS II flight unit are presented in Figure 10. This procedure was repeated at different temperatures.

During the mission, the magnetite CCT (Compositional Calibration Target) will be measured in several runs to verify the functionality of MIMOS II. The well known Mössbauer parameters of magnetite can be used for velocity calibration again. These kind of measurements have been done already in the lab with the flight units as a function of temperature, to be used as reference for the measurements on Mars. Figure 11 shows a "raw" 512 channel Mössbauer spectrum for the CCT.

The primary method for velocity calibration is the internal reference target and detector configured in transmission measurement geometry (Figures 5 and 6). The reference target is a mixture of α-Fe^0 (metallic iron, 30% enriched ^{57}Fe) and α-Fe_2O_3 (hematite, 95% enriched ^{57}Fe), and its Mössbauer spectrum is measured automatically during each backscattering measurement. Each component of the reference target has well-known Mössbauer parameters, so that fitting of reference spectra enables velocity calibration for each individual measurement done in backscatter geometry, ensuring that the actual drive velocity is always well-defined, regardless of prevailing environmental conditions.

3.7.2 Detector calibration. Careful energy calibration on each detector was done to achieve optimal detection rate. Each sensor head was temperature cycled (153 K – 293 K).

During cycling, energy spectra were measured. As a result of analysis of these spectra, optimal firmware parameters were calculated for each detector and each temperature window. During operation, instrument firmware will adjust those parameter depending on temperature, thus ensuring best detector performance.

4. Validation of MIMOS II Performance

In this section, we compare MIMOS II and laboratory Mössbauer spectra and parameters derived from those spectra to document the performance of MIMOS II. We also report initial measurements to determine the detection limit of the instrument for silicate and oxide phases against palagontic tephra, a Martian bright regions analogue [*Morris et al.,* 2000].

Figure 12 shows Mössbauer spectra (293 K) for five Martian analogue samples obtained in transmission geometry using a laboratory spectrometer and in backscatter geometry using a prototype MIMOS II instrument. The MIMOS II spectra are 512 channels of mirror-imaged spectra folded to 256 channels. The laboratory spectra are 1024 channels of mirror imaged spectra folded to 512 channels [e.g., *Morris et al*., 2000]. For purposes of comparison, the laboratory spectra were inverted and overlaid on the backscatter spectra. The backscatter and inverted transmission spectra nearly exactly coincide. In particular, note that peaks in the backscatter spectra are not skewed away from zero velocity relative to the corresponding peaks in the transmission spectra and that the corresponding relative peak heights are approximately the same. These two observations show that cosine smearing may not be a significant or even detectable consideration for MER backscatter spectra and that theoretical peak intensity ratios in transmission measurements (e.g., 3:2:1:1:2:3 for sextets) are applicable for backscatter measurements, at least for these kinds of samples.

Mössbauer spectra for two reference rock slabs are shown in Figure 13, and the derived Mössbauer parameters are given in Table 1. The Mössbauer parameters for AREF043 and AREF121 are consistent with literature values for magnetite and hematite, respectively [e.g., *Stevens et al*., 1998], and these two oxides are the only iron bearing phases detected in these two rock samples. The AREF043 spectrum was acquired in 49 hours with a 25 mCi source intensity. This is the equivalent of a 12 hour integration at the nominal source intensity at Mars during the MER mission. The AREF121 spectrum was acquired in 92 hours with a source activity of 30 mCi, corresponding to about 27 hr at 100 mCi (nominal at Mars). This is a higher quality

spectrum than will likely be obtained on Mars. Note that the Mössbauer parameters that are calculated with and without inclusion of cosine smearing are nearly the same, implying that cosine smearing can be to first order ignored for spectra obtained with MIMOS II.

To estimate detection limits for various Mars-relevant iron-bearing phases, we mixed (by ultrasonic dispersal in ethanol followed by air drying) various quantities of those phases (e.g., hematite, goethite, and olivine) with the <150 μm size fraction of palagonitic tephra HWMK600, which is a Martian bright regions spectral analogue [*Morris et al.*, 2000]. Figure 14 shows Mössbauer spectra obtained by an engineering model MIMOS II for mixtures of the palagonite with well-characterized submicron powders [*Morris et al*., 1985] of hematite (HMS3 and HMS12) and magnetite (MTS4). Although additional measurements are needed (for both oxide and silicate phases) at different mixing ratios, 10 hr integrations (comparable to overnight experiments on Mars) at a source intensity of ~80-100 mCi are sufficient of detect hematite and magnetite at the 1-2% level against a background of palagonitic tephra.

5. Operational Considerations

5.1 Planned Measurements

The instruments on the Athena payload [*Squyres et al.*, this issue] were chosen to be complementary to one another, and wherever possible the targets analyzed by the Mössbauer Spectrometer will be examined by all the other instruments on the payload as well. There is particular synergy between the MIMOS II and the APXS. Both these IDD-mounted instruments will be normally operated during the overnight period, with the split in analysis time depending on the information available on the target. The APXS provides the elemental composition for the target, and MIMOS II provides the mineralogical composition, including the Fe^{2+}/Fe^{3+} ratio so that concentrations of FeO and Fe_2O_3 can be include in the major element analyses. Images of the target, taken before and after MIMOS II and APXS measurements, by the Microscopic Imager (MI; *Herkenhoft et al*., this issue) document the material actually analyzed. Images taken by the front Hazcams [*Maki et al*., this issue] document instrument placement on the target. Images and multispectral data obtained by Pancam [*Bell et al.*, this issue] and Mini-TES [*Christensen et al.*, this issue] complete full characterization of the target by the Athena instrument suite.

Targets for Mössbauer analysis for the mineralogical composition of Fe-bearing phases, the relative distribution of Fe and its oxidation states among those phases, are the exposed surfaces of soil and rock, interior regions of rock exposed by the Rock Abrasion Tool (RAT [*Gorevan et al.,* this issue]), subsurface soil exposed by trenching [*Arvidson et al*., this issue], and the two magnets mounted on the rover deck [*Madsen et al.* this issue]. In the case of the magnets, it is know from Viking [e.g., *Hargraves*, 1979] and Mars Pathfinder [e.g., *Hviid et al*., 1997; *Madsen et al.*, 1999] that Martian aeolian dust is magnetic, but the composition of the magnetic phase or phases is not known. When the dust buildup on the magnets is sufficiently large, as determined using Pancam, the IDD will be used to place MIMOS II directly against the magnets, providing what should be a definitive identification of the magnetic phases present. Fine-grained material produced by the RAT, if present in sufficient lateral extent and depth, provides a target that is representative of the volume excavated and for which orientation effects are likely not present. The relatively high penetration depth of the 14.4 keV Mössbauer radiation (Figures 3 and 4) means that it may be possible to obtain mineralogical information about unaltered rock without removing exterior rinds or dust coverings with the RAT.

The Mössbauer is a less contamination sensitive to dust than the APXS [*Rieder et al*., this issue] or the Microscopic Imager [*Herkenhoff et al*., this issue], which are the other two instruments on the IDD. Therefore, for soft and/or dirty targets the MIMOS II contact sensor may sometimes be used as a "blind man's cane", helping to establish target location in IDD coordinates so that the other instruments can be placed with less risk of contamination.

In some instances, it may be possible for MIMOS II to achieve a signal-to-noise ratio that is adequate for answering key scientific questions in a time much less than the nominal experiment time of 6-12 hr during the overnight period. This will be particularly true early in the mission when radiation source strength is greatest, and for targets with high Fe contents. Where appropriate, then, the Mössbauer may be used in a "touch and go" mode [*Squyres et al*., this issue], in which a short integration is performed at the start of a sol, followed by other rover activities that may include driving.

5.2 Data Analysis

For a Mössbauer experiment on any target, MIMOS II stores in memory for return to the Earth the following information: (1) a PHA spectrum for each of the 5 detectors; (2) five

Mössbauer spectra (one reference and four sample spectra) for each of the 13 temperature intervals for a total of 65 spectra; (3) reference and sample temperatures; and (4) engineering data (e.g., the error signal for the velocity transducer). The Mössbauer spectra are in counts per channel for 512 channels. In (2), the four sample Mössbauer spectra in each temperature interval can selected in a number of ways. For example, they can be the 14.4 keV spectrum from each of the four detectors or the sum of the 14.4 and 6.4 keV spectra for each of the four detectors. Alternatively, the four spectra can be 14.4 and 6.4 keV spectra, each summed over two detectors. The spectra can be analyzed individually or combined to produce higher quality spectra. Combining spectra from different temperature intervals will depend on how strongly the spectra depend on temperature.

Linear least squares spectral fitting routines (developed by our team) will be used to calculate Mössbauer parameters from the spectra. Normally, the velocity axis is calibrated using the spectra from the hematite plus α-Fe^0 reference absorber. The velocity locations of the peaks in the reference spectrum are accurately known through measurements as a function of temperature on Earth and measurement of the reference temperature during measurements on Mars. As a backup, the MIMOS II can also be calibrated against the magnetite CCT target. The fitting routines employ Lorentzian and other lineshape functions and have integrated cosine smearing routines.

For phase identification, the most extensive source of Mössbauer parameters (including measurements at different temperatures) is the Mössbauer Information System (MIS) of the Mössbauer Effect Data Center (MEDC) at the University of North Carolina at Ashville. The MEDC is a scientific center collecting Mössbauer data since the discovery of the Mössbauer effect. The MIS contains about 30,000 bibliographic references, and updates are regularly published in the volumes of Mössbauer Effect Reference and Data Journal (MERDJ). One MERDJ volume contains 10 issues and a special index, covering one year of literature search. For our real-time database during mission operations, we have assembled from the literature a database of Mössbauer parameters (IS, QS, and B_{hf}), main site substitution, and behavior as a function of temperature for ~500 individual mineral phases. In addition, we also have Mössbauer spectra for over 1000 Martian analogue samples along with (incomplete) supporting chemical, magnetic, thermal emissivity, X-ray diffraction, and visible and near-IR spectral data. An implemented artificial neural network system was trained with our compiled database and will be

used for quick mineral identification from measured Mössbauer parameters [*de Souza,* 1999, 2001].

Acknowledgements. The development and realization of MIMOS II was funded by the German Space Agency DLR under contract 50QM 99022. The project has been supported by the Universities of Darmstadt and Mainz. P.A.deS. acknowledges the support for this project of CAPES and CVRD from Brasil. R.V.M. acknowledges the support of the MER Project of the National Aeronautics and Space Administration. The support of the Russian space agency is acknowledged.

References

Agresti, D.G., R. V. Morris, E.L. Wills, T. D. Shelfer, M. M. Pimperl, M. Shen, B. C. Clark, B. D. Ramsey, Extraterrestrial Mössbauer Spectrometry, *Hyp. Int. 72,* 285-298. 1992.

Aramu, F., and V. Maxia, Shift and broadening of Mössbauer peaks by lack of collimation. *Nucl. Instr. and Met*h. 80, 35-39, 1970.

Arvidson R.E., C. Acton, D. Blaney, J. Bowman , S. Kim, G. Klingelhoefer, J. Marshall, C. Niebuhr, J. Plescia, S. Saunders, and C.T. Ulmer. Rocky 7 prototype Mars rover field geology experiments 1. Lavic Lake and Sunshine Volcanic Field, California, *J. Geophys. Res., 103,* 22,671-22,688, 1998.

Arvidson, R. E., R. C. Anderson, A. F.C. Haldemann, G. Landis, R. Li, R. Lindemann, J. Matijevic, R. V. Morris, L. Richter, S. W. Squyres, R. Sullivan, N. Snider, Physical properties and localization investigations associated with the 2003 Mars Exploration Rovers, J. Geophys. Res., this issue.

Bancroft, G. M., *Mössbauer Spectroscopy. An Introduction for Inorganic Chemists and Geochemists*, McGraw Hill, New York, 1973.

Bell III, J. F., R. V. Morris, and J. B. Adams, Thermally altered palagonitic tephra: A spectral and process analog to the soil and dust of Mars, *J. Geophys. Res.*, *98*, 3373-3385, 1993.

Bell III, J. F., S. W. Squyres, K. E. Herkenhoff, J. N. Maki, M. Schwochert, A. Dingizian, M. Wadsworth, S. T. Elliot, D. Brown, R. V. Morris, H. M. Arneson, M. J. Johnson, A.G. Hayes, J. Joseph, J. N. Sohl-Dickstein, R. Sullivan, M. T. Lemmon, W. T. Sullivan, J. R. Johnson, K. Kinch, and G. H. Smith, The Mars Exploration Rover Athena panoramic camera (Pancam) investigation, *J. Geophys. Res.*, this issue.

Bishop, J. L., C. M. Pieters, and R. G. Burns, Reflectance and Mössbauer spectroscopy of ferrihydrite-montmorillonite assemblages as Mars soil analog materials, *Geochim. Cosmochim. Acta*, *57*, 4583-4595, 1993.

Bishop, J. L., C. M. Pieters, R. G. Burns, J. O. Edwards, R. L. Mancinelli, and H. Froschel, Reflectance spectroscopy of ferric sulfate-bearing montmorillonites as Mars soil analogue materials, *Icarus*, *117*, 101-119, 1995.

Bishop, J. L. and E. Murad, Schwertmannite on Mars? Spectroscopic analyses of schwertmannite, its relationship to other ferric minerals, and its possible presence in the surface material on Mars, in *Mineral Spectroscopy: A Tribute to Roger G. Burns*, edited by M. D. Dyar, C. McCammon, and M. W. Schaefer, pp. 337-358, The Geochemical Society, Special Publication No. 5, Houston, 1996.

Burns, R. G., Mössbauer spectral characterization of iron in planetary surface materials, in *Remote Geochemical Analysis: Elemental and Mineralogical Composition*, edited by C. M. Pieters and P. A. J. Englert, pp. 539-556, Cambridge University Press, Cambridge, 1993.

Burns, R. G., and D. S. Fisher, Iron-sulfur mineralogy of Mars: Magmatic evolution and chemical weathering products, *J. Geophys. Res.*, *95*, 14,415-14,421, 1990.

Burns, R. G., and S. L. Martinez, Mössbauer spectra of olivine-rich achondrites: Evidence for preterrestrial redox reactions, *Proc. Lunar Planet. Sci. Conf. 21*, 331-340, 1991.

Burns, R. G., and T. C. Solberg, ^{57}Fe-bearing Oxide, Silicate, and Aluminosilicate Minerals, Crystal Structure Trends in Mössbauer Spectra, in Spectroscopic Characterization of Minerals and Their Surfaces, pp. 262-283, American Chemical Society, Washington, D. C., 1990.

Christensen, P. R., J. L. Bandfield, R. N. Clark, S. Edgett.K, V. E. Hamilton, T. Hoefen, H. H. Kieffer, R. O. Kuzmin, M. D. Lane, M. C. Malin, R. V. Morris, J. C. Pearl, R. Pearson, T. L. Roush, S. W. Ruff, and M. D. Smith, Detection of crystalline hematite mineralization on Mars by the Thermal Emission Spectrometer, *J. Geophys. Res.*, *105*, 9623-9642, 2000.

Christensen, P. R., R. V. Morris, M. D. Lane, J. L. Bandfield, and M. C. Malin, Global mapping of Martian hematite mineral deposits: Remnants of water-driven processes on early Mars, *J. Geophys. Res.*, *106*, 23,873-23,885, 2001.

Christensen, P. R. et al., Miniature Thermal Emission Spectrometer, *J. Geophys. Res.*, this issue.

De Grave, E. and A. Van Alboom, Evaluation of ferrous and ferric Mössbauer fractions, Phys. Chem. Minerals, 18, 337-342, 1991.

De Souza Jr., P. A., *Automation in Mössbauer Spectroscopy Analysis,* Laboratory Robotics and Automation, Vol.11, no.1, 13-23, 1999.

De Souza Jr., P.A. and G. Klingelhöfer, *Mars-Analogue Minerals, Soils, and Rocks studied by Mössbauer Spectroscopy,* Meteoritics and Planetary Science, Vol. 36A, 139, 2001.

Evlanov , E.N., V.A. Frolov, O.F. Prilutski, A.M. Rodin, G.V. Veselova, and G. Klingelhöfer, *Mössbauer Spectrometer for Mineralogical Analysis of the Mars Surface: Mössbauer Source Considerations*, Lunar and Planetary Science XXIV, 459-460, 1993

Fegley Jr., B., G. Klingelhöfer, R. A. Brackett, N. Izenberg, D. T. Kremser, and K. Lodders, Basalt oxidation and the formation of hematite on the surface of Venus*, Icarus, 118*, 373-383, 1995

Fernandez-Moran, H., S. S.Hafner, M. Ohtsuki, D. Virgo, Mössbauer Effect and High-Voltage Electron Microscopy of Pyroxenes in Type B Samples, *Science 167*, 686-688. 970.

Galazkha-Friedman, J., and J. Juchniewicz, *Martian Mössbauer Spectrometer MarMös,* Project Proposal, Space Research Center, Polish Academy of Sciences, February, 1989.

Gay, P., G. M.Bancroft, and M. G.Bown, Diffraction and Mössbauer Studies of Minerals from Lunar Soils and Rocks, *Science, 167*, 626-628. 1970.

Golden, D. C., R. V. Morris, H. V. Lauer Jr., and S. R. Yang, Mineralogy of three slightly palagonitized tephra samples from the summit of Mauna Kea, Hawaii, *J. Geophys. Res.*, *98*, 3401-3411, 1993.

Gonser, U., Mössbauer Spectroscopy, in *Microscopic Methods in Metals,* Chapter 13, edited by U. Gonser, pp. 409-448, Springer Verlag, New York, 1986.

Gonser, U., F. Aubertin, S. Stenger, H. Fischer, G. Smirnov, and G. Klingelhöfer, Polarization and Thickness Effects in Mössbauer Spectroscopy*, Hyperfine Interactions, 67*, 701-710, 1991.

Gorevan, S, The Rock Abrasion Tool, Mars Exploration Rover Mission, *J. Geophys Res*., this issue.

Graff, T. G., R. V. Morris, and P. R. Christensen, Lunar mare basalts as analogues for Martian volcanic compositions: Evidence from visible, near-IR, and thermal emission spectroscopy. In *Lunar and Planetary Science XXXIV*, Abstract #1632, Lunar and Planetary Institute, Houston (CD-ROM), 2003.

Greenwood, N. N. and T. C. Gibb, *Mössbauer Spectroscopy*, Chapman and Hall Ltd, London, 1971.

Gummer, A.W., Effect of accumulated Decay Product on the Mössbauer Emission Spectrum, *Nucl.Inst.Meth. B34*, 224-227. 1988

Hargraves, R. B., D. W. Collinson, R. E. Arvidson, and P. M. Cates, Viking magnetic properties experiment: Extended mission results, *J. Geophys. Res.*, *84*, 8379-8384, 1979.

Hawthorne, F. C., Mössbauer Spectroscopy, in *Reviews in Mineralogy,* Volume 18: Spectroscopic Methods in Mineralogy and Geology, edited by F. C. Hawthorne, pp. 255-340, Mineralogical Society of America, 1988.

Held, P.*, PIN-Photodioden als Detektoren für das Mössbauerspektrometer MIMOS zur Untersuchung der Marsoberfläche*, Diploma Thesis, University Darmstadt, Inst. f. Nuclear Physics, 1993a.

Held, P., R. Teucher, G. Klingelhöfer, J. Foh, H. Jäger, and E. Kankeleit, Mössbauer Spectrometer for Mineralogical Analysis of the Mars Surface: First temperature dependent tests of the detector and drive system, *Lunar and Planetary Science XXIV*, 633-634. 1993b.

Held, P, *MIMOS II: Ein miniaturisiertes Mößbauerspektrometer in Rückstreugeometrie zur mineralogischen Analyse der Marsoberfläche.* PhD Thesis, Institut for Nuclear Physics, UniversityDarmstadt, 1997.

Herkenhoff, K. E., S. W. Squyres, J. F. Bell III, L. A. Soderblom, M. A. Schwochert, D. I. Brown, S. A. Collins, A. Dingizian, S. T. Elliot, E. C. Hagerott, J. Maki, L. Scherr, L. Shiraishi, G. H. Smith, R. L. Kirk, R. V. Morris, H. M. Arneson, A. Hayes, M. J. Johnson, J. Sohl-Dickstein, and the Athena Science Team, The Athena Microscopic Imager Investigation, *J. Geophys. Res*., this issue.

Herzenberg, C. L., R. B. Moler, and D. L. Riley, Mossbauer instrumental analysis of Apollo12 lunar rock and soil samples, *Proc. Lunar Planet. Sci. Conf. 2nd*, 2103-2123, 1971.

Herzenberg, C. L. and D. L. Riley, Analysis of first returned lunar samples by Mossbauer spectrometry, *Proc. Lunar Planet. Sci. Conf 1st*, 2221-2241, 1970.

Housley, R. M., M. Blander, M. Abdel-Gawad, R. W. Grant, and A. H. Muir Jr., Mossbauer spectroscopy of Apollo 11 samples, *Proc. Lunar Sci. Conf. 11th*, 2251-2268, 1970.

Housley, R. M., R. W. Grant, A. H. Muir Jr., M. Blander, and M. Abdel-Gawad, Mossbauer studies of Apollo 12 samples, *Proc. Lunar Planet. Sci. Conf. 2nd*, 2125-2136, 1971.

Housley, R. M., E. H. Cirlin, and R. W. Grant, Characterization of fines from the Apollo 16 site, *Proc. Lunar Planet. Sci. Conf. 4th*, 2729-2735, 1973.

Huffman, G. P., F. C. Schwerer, and R. M. Fisher, Iron distributions and metallic-ferrous ratios for Apollo lunar samples: Mossbauer and magnetic analyses, *Proc. Lunar Planet. Sci. Conf. 5th*, 2779-2794, 1974.

Hviid, S. F., M. B. Madsen, H. P. Gunnlaugsson, W. Goetz, J. M. Knudsen, R. B. Hargraves, P. Smith, D. Britt, A. R. Dinesen, C. T. Morgensen, M. Olsen, C. T. Pedersen, and L. Vistisen, Magnetic properties experiments on the Mars Pathfinder Lander: Preliminary results, *Science*, *278*, 1768-1770, 1997.

Johnson, G. R. and G. R. Olhoeft, Densities of Rocks and Minerals, in *CRC Handbook of Physical Properties of Rocks, Volume III*, edited by R. S. Carmichael, pp. 1-38, CRC Press, Inc., Boca Raton, FL, 1984.

Kankeleit, E., Velocity Spectrometer for Mössbauer Experiments, *Rev.Sci.Instr. 35*, 194-197. 1964.

Kankeleit, E., Some Technical Developments in Mössbauer Spectroscopy, *Proc. Int. Conf. on Mössbauer Spectroscopy*, Vol.2, Cracow, Poland, 43. 1975.

Klingelhöfer, G., U. Imkeller, E. Kankeleit, and B. Stahl, Remarks on depth selective CEMS – backscattering measurements, *Hyp. Int. 71*, 1445-1448, 1992

Klingelhöfer, G., B. Fegley Jr., R. V. Morris, E. Kankeleit, P. Held, and E. P. O. Evlanov, Mineralogical analysis of Martian soil and rock by a miniaturized backscattering Mössbauer spectrometer, *Planet. Space Sci.*, *44*, 1277-1288, 1996.

Klingelhöfer, G., P. Held, B. Bernhardt, J. Foh, R. Teucher, and E. Kankeleit, In-situ phase analysis by a versatile miniaturized Mössbauer spectrometer, *Hyperfine Interactions*, *111*, 331-334, 1998.

Klingelhöfer, G., The miniaturized spectrometer MIMOS II, in *Mössbauer Spectroscopy in Materials Science*, edited by M. Miglierini and D. Petridis, pp. 413-426, Kluwer Academic Publishers, Netherlands, 1999.

Knudsen, J. M., Mössbauer Spectroscopy of ^{57}Fe and the Evolution of the Solar System, *Hyp. Int. 47*, 3-31. 1989.

Knudsen, J.M., S. Moerup, and J. Galazkha-Friedman, *Mössbauer Spectroscopy and the Iron on Mars*, *Hyp.Int. 57*, 2231-2234. 1990.

Knudsen, J. M., M. B. Madsen, M. Olsen, L. Vistisen, C. B. Koch, S. Moerup, E. Kankeleit, G. Klingelhöfer, E. N. Evlanov, V. N. Khromov, L. M. Mukhin, O. F. Prilutskii, B. Zubkov, G. V. Smirnov, and J. Juchniewicz, Mössbauer spectroscopy on the surface of the planet Mars. Why?, *Hyperfine Interactions 68*, 83-94. 1992.

Lane, M. D., R. V. Morris, S. A. Mertzman, and P. R. Christensen, Evidence for platy hematite grains in Sinus Meridiani, Mars, *J. Geophys. Res.*, *107*, 5126, doi: 10.1029/2001JE001832, 2002.

Madsen, M. B., S. Morup, T. V. V. Costa, J. M. Knudsen, and M. Olsen, Superparamagnetic component in the Orgueil meteorite and Mossbauer spectroscopy studies in applied magnetic fields, *Nature*, *29*, 501-503, 1986.

Madsen, M. B., S. F. Hviid, H. P. Gunnlaugsson, J. M. Knudsen, W. Goetz, C. T. Pedersen, A. R. Dinesen, C. T. Morgensen, M. Olsen, and R. B. Hargraves, The magnetic properties experiments on Mars Pathfinder, *J. Geophys. Res.*, *104*, 8761-8779, 1999.

Madsen, M. B. et al., The magnetic properties experiments on Mars, *J. Geophys. Res.*, this issue.

McCammon, C., Mössbauer spectroscopy of minerals, in *Mineral Physics and Crystallography: A Handbook of Physical Constants*, edited by T. J. Ahrens, pp. 332-347, American Geophysical Union, Washington DC, 1995.

Maki, J. et al., The Mars Exploration Rover engineering cameras, *J. Geophys. Res*., this issue.

Morris, R. V., D. G. Agresti, T. D. Shelfer, and T. J. Wdowiak, Mössbauer spectroscopy for mineralogical analysis on planetary surfaces, *SAAP Instrument Technology Workshop, Nov. 14-16, 1988,* Houston TX, 1988.

Morris, R. V., J. J. Gooding, H. V. Lauer Jr., and R. B. Singer, Origins of Marslike spectral and magnetic properties of a Hawaiian palagonitic soil, *J. Geophys. Res.*, *95*, 14,427-14,434, 1990.

Morris, R. V., H. V. Lauer Jr., C. A. Lawson, E. K. Gibson Jr., G. A. Nace, and C. Stewart, Spectral and other physicochemical properties of submicron powders of hematite (α-Fe_2O_3), maghemite (γ-Fe_2O_3), magnetite (Fe_3O_4), goethite (α-FeOOH), and lepidocrocite (γ-FeOOH), *J. Geophys. Res.*, *90*, 3126-3144, 1985.

Morris, R. V., D. G. Agresti, H. V. Lauer Jr., J. A. Newcomb, T. D. Shelfer, and A. V. Murali, Evidence for pigmentary hematite on Mars based on optical magnetic and Mössbauer studies of superparamagnetic (nanocrystalline) hematite, *J. Geophys. Res.*, *94*, 2760-2778, 1989.

Morris, R. V., D. C. Golden, J. F. Bell III, and H. V. Lauer Jr., Hematite, pyroxene, and phyllosilicates on Mars: Implications from oxidized impact melt rocks from Manicouagan Crater, Quebec, Canada, *J. Geophys. Res.*, *100*, 5319-5328, 1995.

Morris, R. V., D. C. Golden, J. F. Bell III, H. V. Lauer Jr., and J. B. Adams, Pigmenting agents in Martian soils: Inferences from spectral, Mössbauer, and magnetic properties of nanophase and other iron oxides in Hawaiian palagonitic soil PN-9, *Geochim. Cosmochim. Acta*, *57*, 4597-4609, 1993.

Morris, R. V., D. W. Ming, D. C. Golden, and J. F. Bell III, An occurrence of jarositic tephra on Mauna Kea, Hawaii: Implications for the ferric mineralogy of the Martian surface, in *Mineral Spectroscopy: A Tribute to Roger G. Burns*, edited by M. D. Dyar, C. McCammon, and M. W. Schaefer, pp. 327-336, The Geochemical Society, Special Publication No. 5, Houston, 1996.

Morris, R. V., D. C. Golden, and J. F. Bell III, Low-temperature reflectivity spectra of red hematite and the color of Mars, *J. Geophys. Res.*, *102*, 9125-9133, 1997.

Morris, R. V., S.W. Squyres, J.F. Bell III, T. Economou, G. Klingelhoefer, P. Held, L.A. Haskin, A. Wang, B.L. Jolliff, and R. Rieder, Analysis of Martian surface materials during the Mars Surveyor 2001 mission by the Athena instrument payload (abstract), *Lunar Planet. Sci. [CD-ROM]*, *XXIX*, abstract 1326, 1998.

Morris, R. V., D. C. Golden, J. F. Bell III, T. D. Shelfer, A. C. Scheinost, N. W. Hinman, G. Furniss, S. A. Mertzman, J. L. Bishop, D. W. Ming, C. C. Allen, and D. T. Britt, Mineralogy, composition, and alteration of Mars Pathfinder rocks and soils: Evidence from multispectral, elemental, and magnetic data on terrestrial analogue, SNC meteorite, and Pathfinder samples, *J. Geophys. Res.*, *105*, 1757-1817, 2000.

Morris, R. V., T.G. Graff, T.D. Shelfer, and J.F. Bell III, Effect of palagonitic dust coatings on visible, near-IR and Mössbauer spectra of rocks and minerals: Implications for mineralogical remote sensing of Mars (abstract), *Lunar Planet. Sci. [CD-ROM]*, *XXXII*, abstract 1912, 2001b.

Morris, R. V., D. C. Golden, D. W. Ming, T. D. Shelfer, L. C. Jorgensen, J. F. Bell III, T. G. Graff, and S. A. Mertzman, Phyllosilicate-poor palagonitic dust from Mauna Kea Volcano (Hawaii): A mineralogical analogue for magnetic martian dust?, *J. Geophys. Res.*, *106*, 5057-5083, 2001a.

Morris, R. V., G. Klingelhofer, R. L. Korotev, and T. D. Shelfer, Mössbauer mineralogy on the Moon: The lunar regolith, *Hyperfine Interactions*, *117*, 405-432, 1998.

Riesenman, R., J. Steger, and E. Kostiner, Cosine Effect in Mössbauer Spectroscopy involving a source of non-zero Radius*, Nucl. Inst. Meth.* 72, 109-110, 1969

Prilutskii, O., Space Research Institute (IKI), Moscow, internal report from Minsk, 1990. Riesenman, R. J. Steger, and E. Kostiner, Cosine effect in Mössbauer spectroscopy involving a source of non-zero radius. *Nucl. Instr. and Meth. 72,* 109-110, 1969.

Schröder C., *Optimierung der Nachweiseigenschaften des miniaturisierten Mössbauer-Spektrometers MIMOS II und Messungen an Mars-Analog-Proben*. Diplomarbeit, Johannes Gutenberg-Universität Mainz, 2001.

Sims, M.R., D. Pullan, G.W. Fraser, S. Whitehead, J. Sykes, J. Holt, G. Butcher, N. Nelms, J. Dowson, D. Ross, C. Bicknell, M. Crocker, B. Favill, A. Wells, L. Richter, H. Kochan, H. Hamacher, L. Ratke, A. Griffiths, A. Coates, N. Phillips, A. Senior, J. Zarnecki, M.C. Towner, M.R. Leese, M. Patel, C. Wilson, N. Thomas, S. Hviid, J.L. Josset, G. Klingelhofer, B. Bernhardt, P. van Duijn, G. Sims, and K.L. Yung, *Performance Characteristics of the PAW Instrumentation on Beagle 2 (The Astrobiology Lander on ESA's Mars Express Mission),* SPIE Proceedings, 4859, 32-44, 2002.

Solberg, T. C. and R. G. Burns, Iron Mossbauer spectral study of weathered Antarctic and SNC meteorites, *Proc. Lunar Planet. Sci. Conf. 19th*, 313-322, 1989.

Squyres, S. W., R. E. Arvidson, E. T. Baumgartner, J. F. Bell III, P. R. Christensen, S. Gorevan, K. E. Herkenhoff, G. Klingelhöfer, M. B. Madsen, R. V. Morris, R. Rieder, and R. A. Romero, The Athena Mars rover science investigation, *J. Geophys. Res.*, this issue.

Stevens, J. G., A. M. Khasanov, J. W. Miller, H. Pollak, and Z. Li (Eds.), *Mössbauer Mineral Handbook*, 527 pp., Biltmore Press, Ashville, NC, 1998.

Straub, D. W., R. G. Burns, and S. F. Pratt, Spectral signature of oxidized pyroxenes: Implications to remote sensing of terrestrial planets, *J. Geophys. Res.*, *96*, 18819-18830, 1991.

Teucher, R., *Miniaturisierter Mössbauerantrieb*, Diploma Thesis, University Darmstadt, Inst. f. Nuclear Physics, 1994

Vieira, V. W. A., T. V. V. Costa, H. G. Jensen, J. M. Knudsen, and M. Olsen, Oxidation state of iron in SNC meteorites as studied by Mössbauer spectroscopy, *Physica Scripta*, *33*, 180-186, 1986.

Wade, M. L., D. G. Agresti, T. J. Wdowiak, and L. P. Armendarez, A Mössbauer investigation f iron-rich terrestrial hydrothermal vent systems: Lessons for Mars exploration, *J. Geophys. Res.*, *104*, 8489-8507, 1999.

Wdowiak, T. J. and D. G. Agresti, Presence of a superparamagnetic component in the Orgueil meteorite, *Nature*, *311*, 140-142, 1984.

Weinheimer, Ch., M. Schrader, J. Bonn, Th. Loeken and H. Backe, Measurement of energy resolution and dead layer thickness of LN2-cooled PIN photodiodes, *Nucl. Inst. Meth. A311,* 273-279. 1992.

Wertheim, G. K., *Mössbauer Effect: Principles and Applications*, Academic Press, New York, 1964.

Table 1. Mössbauer parameters (293 K) for spectra in Figure 13.

	IS, mm/s	QS, mm/s	B_{hf} T
Fits using Lorentzian lineshapes with cosine smearing correction			
AREF043			
oct-(Fe^{2+},Fe^{3+})	0.665(2)[a]	0.002(1)	45.82(2)
tet-Fe^{3+}	0.282(3)	-0.002(3)	49.00(2)
AREF121, oct-Fe^{3+}	0.377(1)	-0.198(1)	51.58(1)
Fits using pure Lorentzian lineshapes			
AREF043			
oct-(Fe^{2+},Fe^{3+})	0.666(1)	0.001(3)	46.09(7)
tet-Fe^{3+}	0.294(2)	0.012(4)	49.43(2)
AREF121, oct-Fe^{3+}	0.379(1)	-0.199(1)	51.96(1)

[a]Numbers in parenthesis are the statistical error according to the chi-squared fit.

Figure Captions

Figure 1. Energy level diagram for ^{57}Fe in showing singlet emission of 14.4 keV γ-rays from the Mössbauer source and absorption of the γ-rays in three different nuclear environments.

Figure 2. Schematic illustration of the measurement geometry for Mössbauer spectrometers. In transmission geometry, the absorber (sample) is between the nuclear source of 14.4 keV γ-rays (normally $^{57}Co/Rh$) and the detector. The peaks are negative features, and the absorber should be "thin" with respect to absorption of the γ-rays to minimize non-linear effects. In emission (backscatter) Mössbauer spectroscopy, the radiation source and detector are on the same side of the sample. The peaks are positive features, corresponding to recoilless emission of 14.4 keV γ-rays and conversion X-rays and electrons. For both measurement geometries, Mössbauer spectra are counts per channel as a function of the Doppler velocity (normally in units of mm/s relative to the mid-point of the spectrum of α-Fe^0).

Figure 3. Calculated relationship between the thickness of an alteration rind and/or dust coating on a rock and the amount of 15.0-keV radiation absorbed in the rind/coating for densities of 0.4, 2.4, and 4.0 g/cm^3 (after *Morris et al*. [2000]). The bulk chemical composition of basaltic rock was used in the calculations, and the 15.0 keV every is approximately the energy of the 14.4 keV γ-ray used in the Mössbauer experiment. The stippled area between densities of 2.4 and 4.0 g/cm^3 is the region for dry bulk densities of terrestrial andesitic and basaltic rocks [*Johnson and Olhoeft*, 1984]. The stipples area between densities of 0.1 and 0.4 g/cm^3 corresponds approximates the range of densities possible for Martian dust. The density of 0.1 g/cm^3 is the density of basaltic dust deposited by air fall in laboratory experiments [*Morris et al.*, 2001b].

Figure 4. Demonstration of the depth selective surface analysis for a sandwich of α-Fe^0, aluminum, and stainless steel (SS) foils. In transmission geometry, only the 14.4 keV γ-rays can be measured. In backscatter geometry, both the 6.4 keV X-rays and 14.4 keV γ-ray can be measured. For backscatter measurement geometry, note that the 6.4 keV X-rays are detected only from the α-Fe^0 foil and that the 14.4 γ-rays are detected from both the α-Fe^0 and SS foils.

Figure 5. Schematic drawing of the MIMOS II Mössbauer spectrometer. The velocity transducer to which both the reference and main ^{57}Co/Rh sources are attached is shown in detail. The transmission spectrum for a prototype internal reference standard shows the peaks corresponding to hematite (α-Fe_2O_3), α-Fe^0, and magnetite (Fe_3O_4). The internal reference standards for MIMOS II flight units are only hematite and metallic iron. The backscatter spectrum for the magnetite MER compositional calibration target (CCT), which is mounted on the rover deck and is available to the MIMOS II during the mission, is also shown.

Figure 6. (a) External view of the MIMOS II sensor head without contact plate assembly. (b) Mimos II sensor head (without contact plate assembly) with dust cover taken off to show sensor head interior. At the front, the end of the cylindrical collimator is surrounded by the four Si-PIN detectors that detect the radiation emitted by the sample. The metal case of the upper detector is removed to the show its associated electronics. The electronics for all four detectors is the same. The Mössbauer drive is inside (in the center) of this arrangement, and the reference channel is located on the back side in the metal box shown in the photograph. (c) View of the MIMOS II sensor head mounted on the turret with the ASI contact plate assembly.

Figure 7. Transfer function for MIMOS II velocity transducer.

Figure 8. Pulse-height analysis (PHA) spectrum for ^{57}Co/Rh backscattered from aluminum and stainless steel plates.

Figure 9. (a) Backscatter MIMOS II spectra collected in eight temperature intervals on the CCT target during a simulated overnight Mössbauer experiment on Mars. (b) Corresponding transmission spectra for the velocity reference sample.

Figure 10. Preflight MIMOS II sensor head velocity calibration.

Figure 11. Representative MIMOS II Mössbauer spectrum of the magnetite CCT target measured for 2 hours at a source intensity of about 200 mCi.

Figure 12. Comparison of Mössbauer spectra (293 K) in backscatter and transmission geometries for Martian analogue samples. Backscatter spectra (512 velocity channels folded to 256 channels) were obtained using a prototype MIMOS II spectrometer, and transmission spectra (1024 velocity channels folded to 512channels were obtained using a laboratory spectrometer. The overlay was done by inverting the transmission spectra, overlapping the baselines, and normalizing maximum intensities to the same value. HWMK600 and HWMK24 are the <1 mm size fractions of palagonitic and jarositic tephra from Mauna Kea Volcano (Hawaii). AKB-1 and BCS-301 are an amygdaloidal basalt (Michigan) and an iron ore (Lincolnshire, England). MAN-74-342A is an impact melt rock from Manicougan Crater (Quebec, Canada). Mössbauer spectra are adapted from *Morris et al.* [1995, 1996, 1998, 2000].

Figure 13. Mössbauer spectra (512 data channels folded to 256 channels) obtained at 293 K using an engineering-model MIMOS II spectrometer for rock slabs AREF043 and AREF121. The experiment time and source intensity for AREF043 were 49 hr and 25 mCi, which corresponds to a 12 hr integration at the Martian source intensity (~100 mCi). The Mössbauer parameters derived from the fits indicate that the iron-bearing phases in AREF043 and AREF121 are magnetite and hematite, respectively. Spectrum AREF043 is magnetite with cosine smearing correction applied while fitting. Spectrum AREF121 of hematite shows the difference between a fit with and without correction for cosine smearing (red and green line respectively).

Figure 14. Mössbauer spectra (512 data channels folded to 256 channels) obtained at 293 K using an engineering-model MIMOS II spectrometer for mixtures of palagonitic tephra HWMK600 (<150 μm) and hematite HMS3 and HMS12 and magnetite MTS4. Experiment times were 10 h.

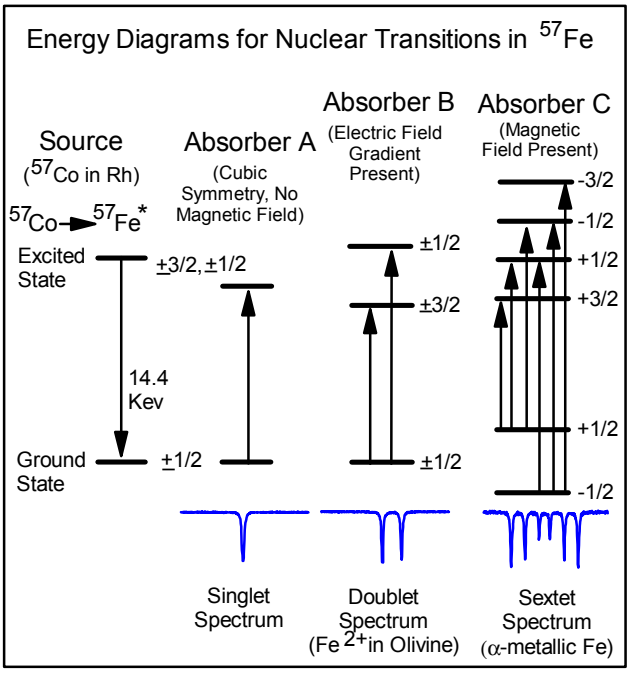

Figure 1, Klingelhoefer et al. [2003]

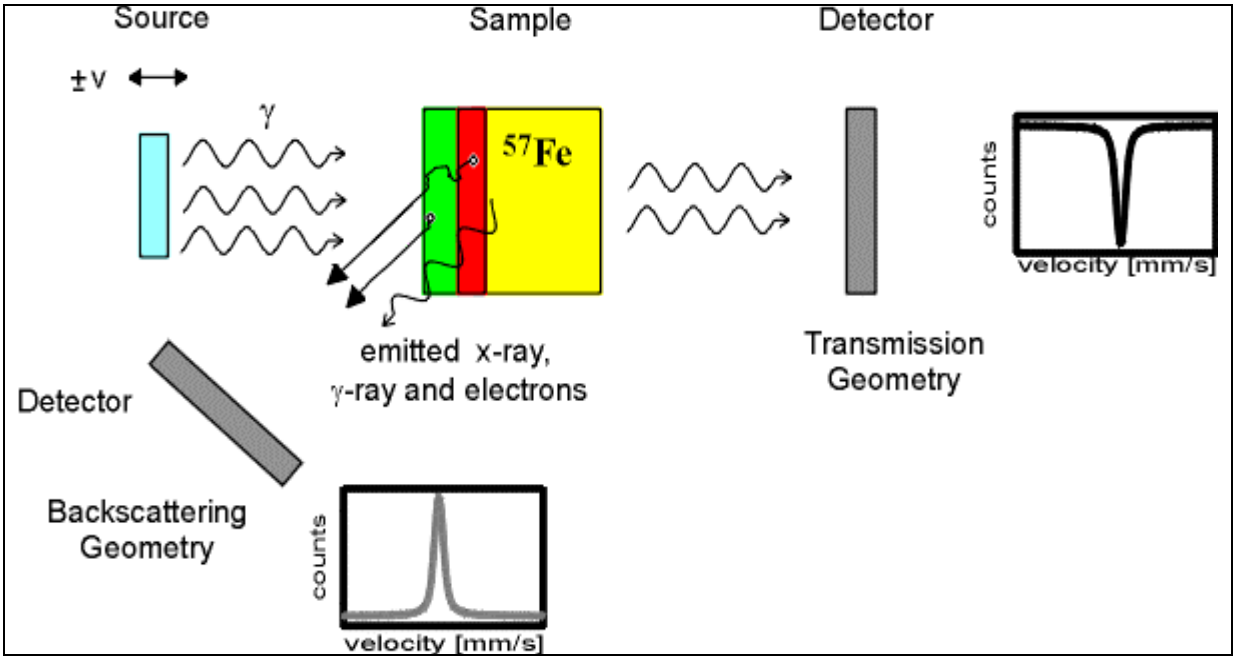

Figure 2. Klingelhoefer et al. [2003]

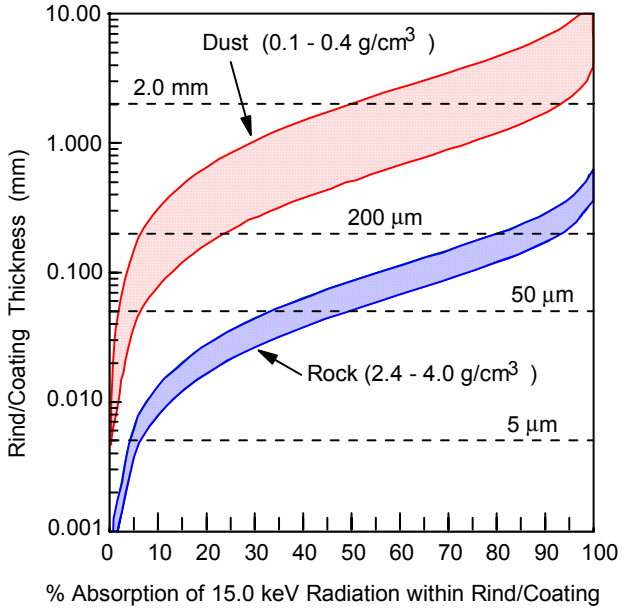

Figure 3, Klingelhoefer et al. [2003]

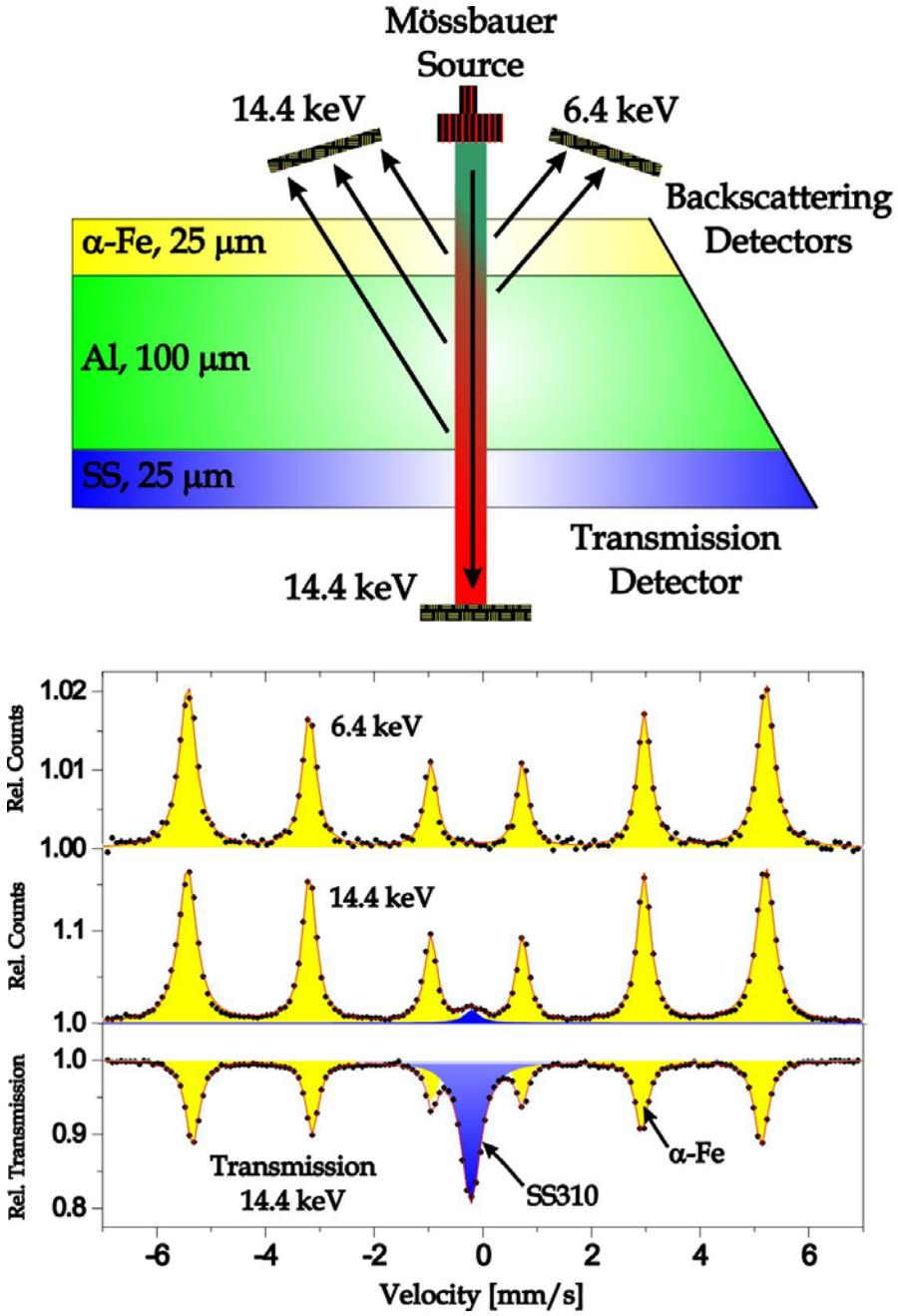

Figure 4, Klingelhoefer et al [2003]

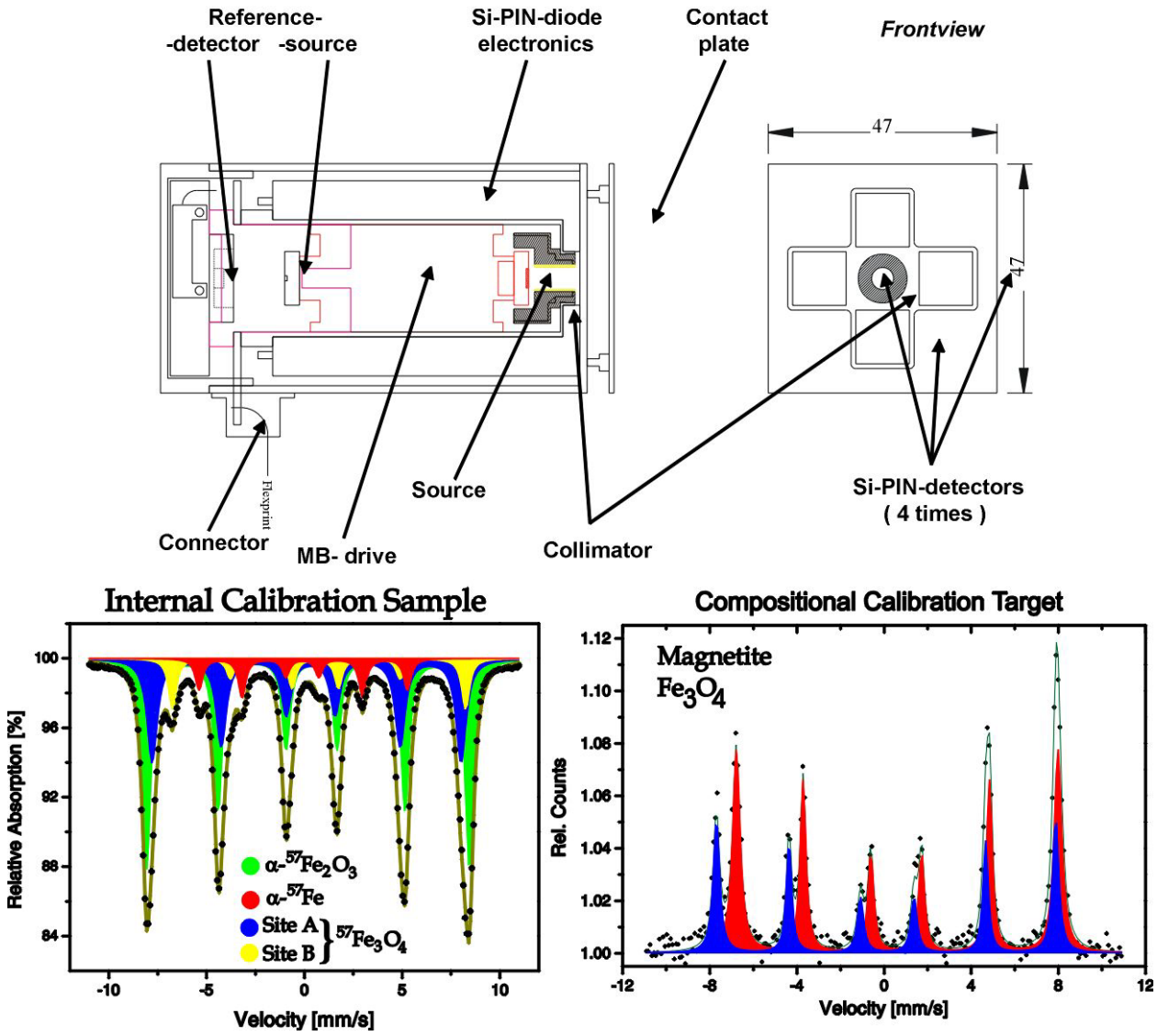

Figure 5. Klingelhoefer et al. [2003].

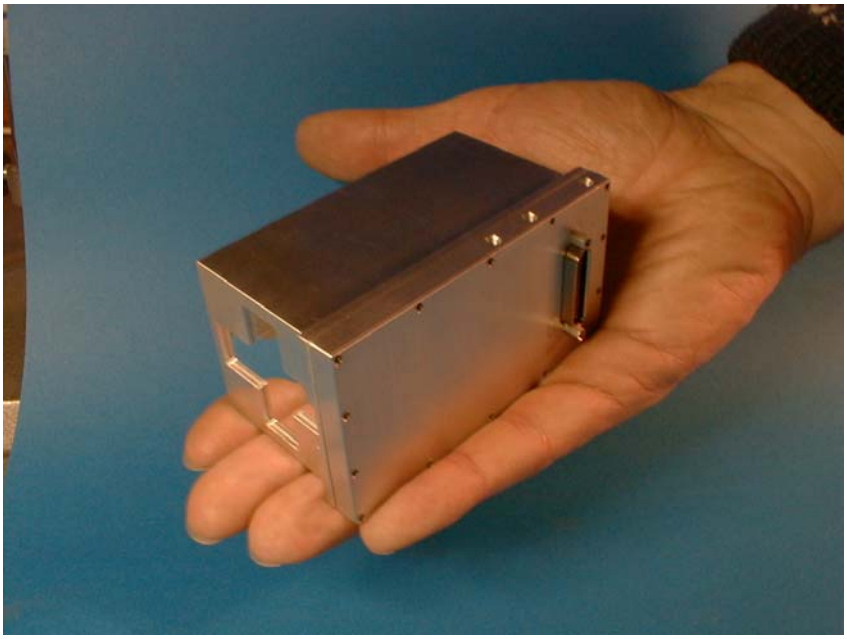

Figure 6a, Klingelhoefer et al. [2003]

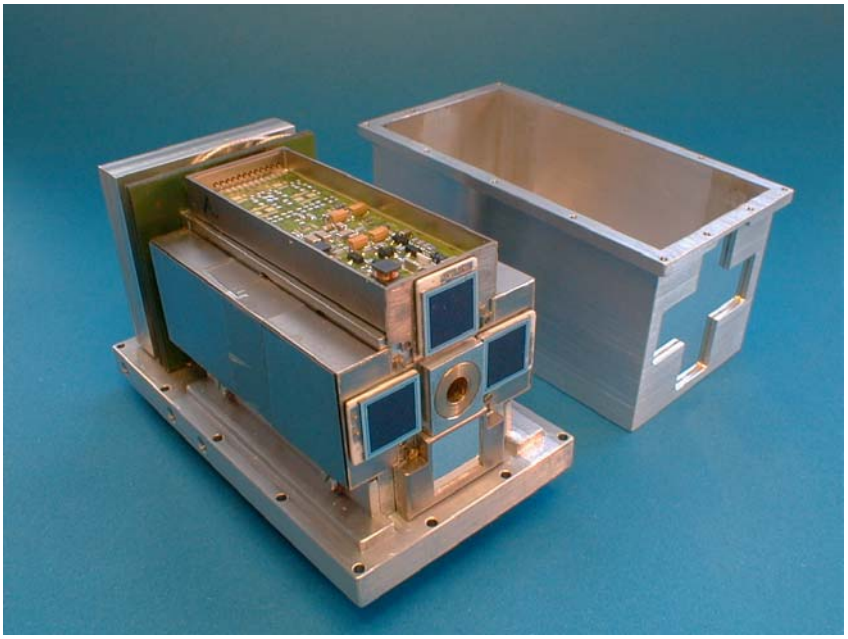

Figure 6b, Klingelhoefer et al. [2003]

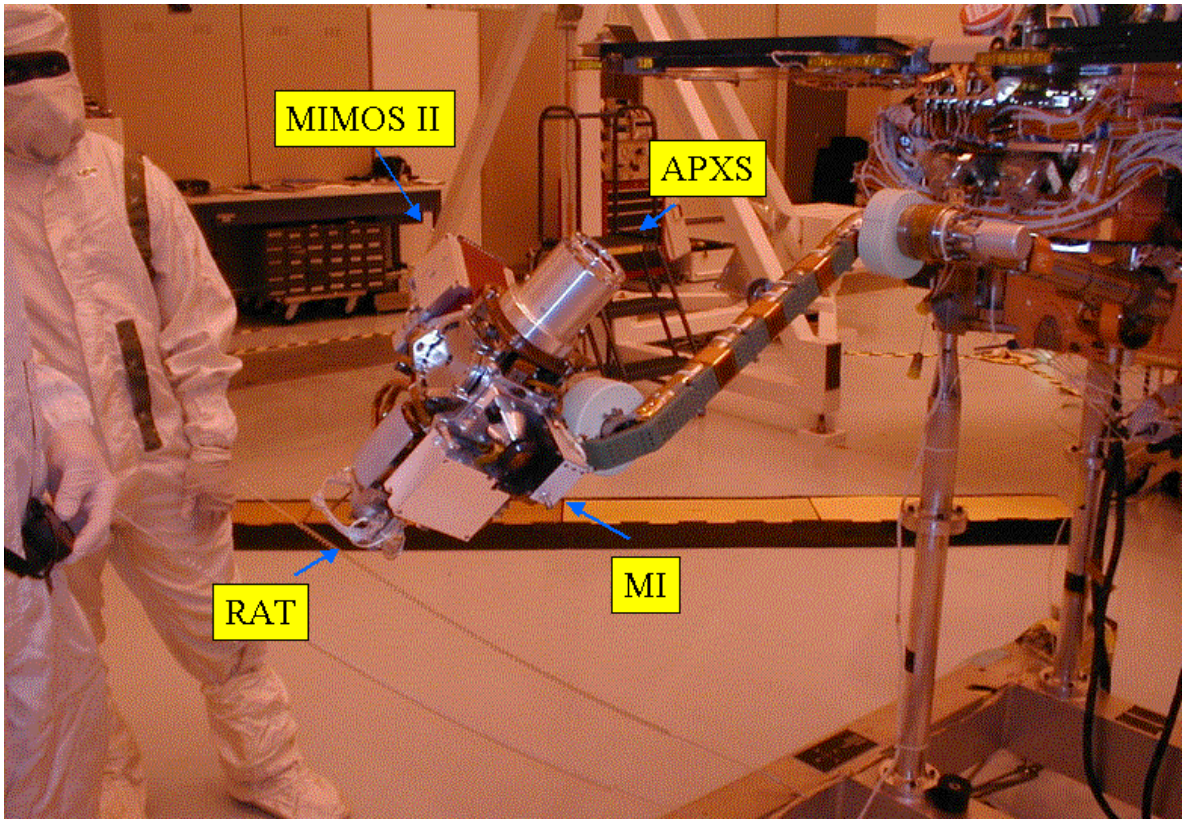

Figure 6c, Klingelhoefer et al [2003].

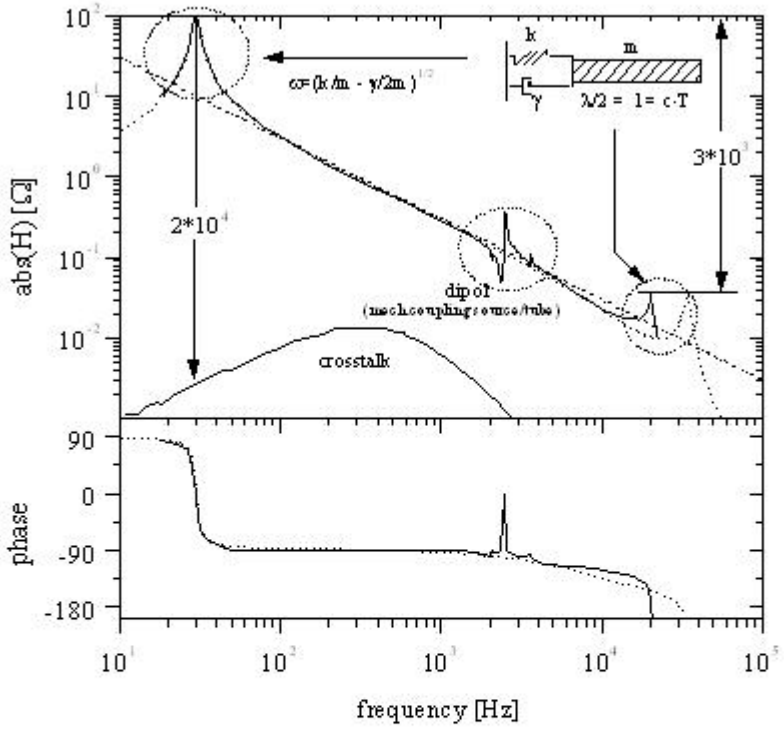

Figure 7, Klingelhoefer et al. [2003]

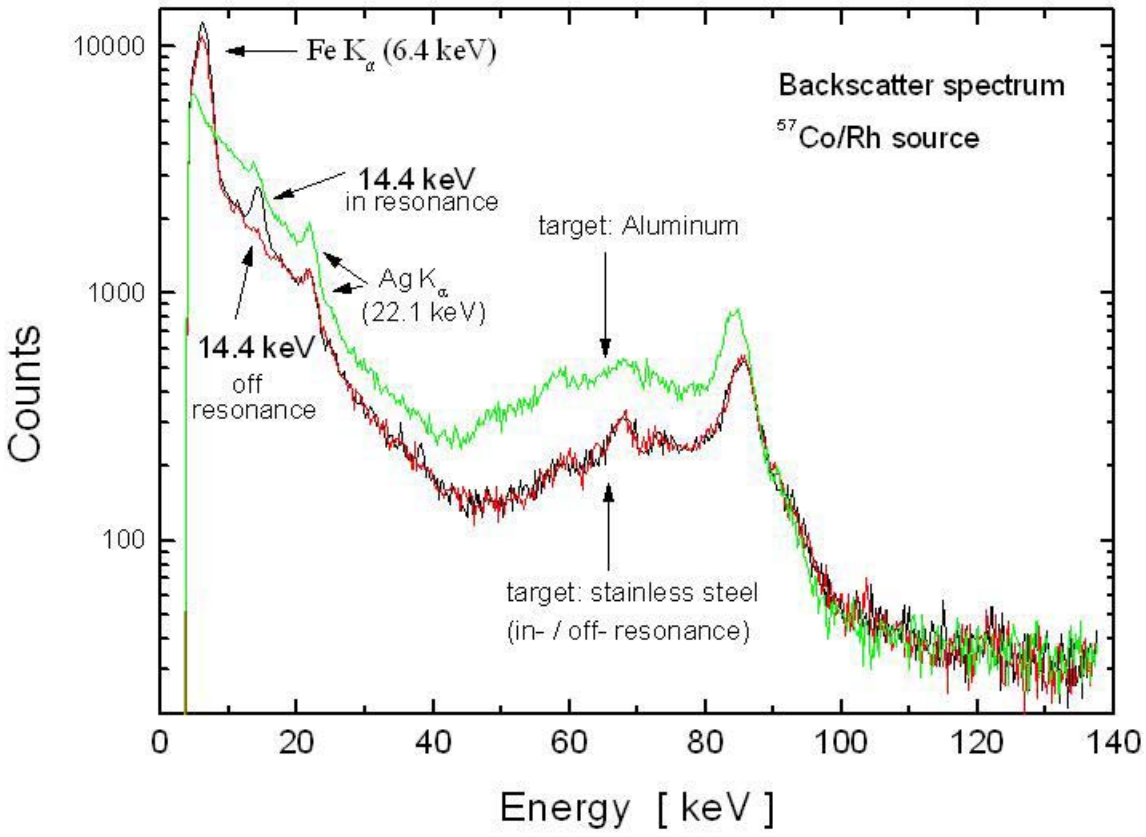

Figure 8, Klingelhoefer et al. [2003

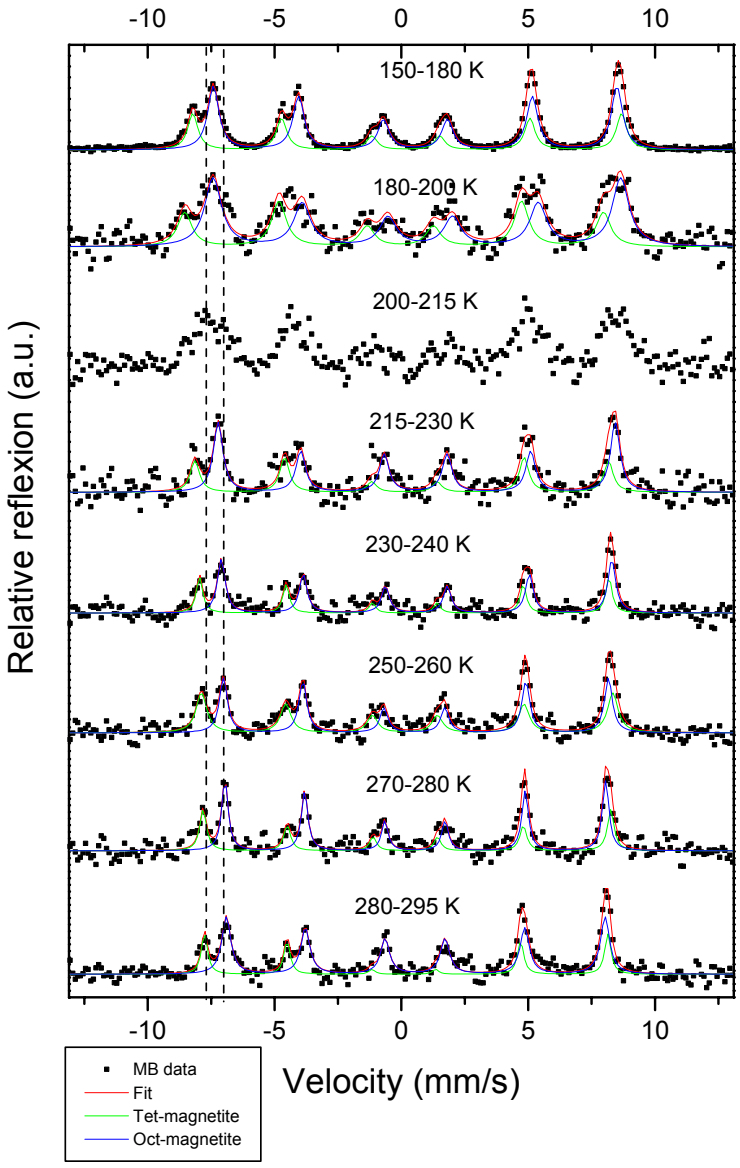

Figure 9a, Klingelhoefer et al. [2003]

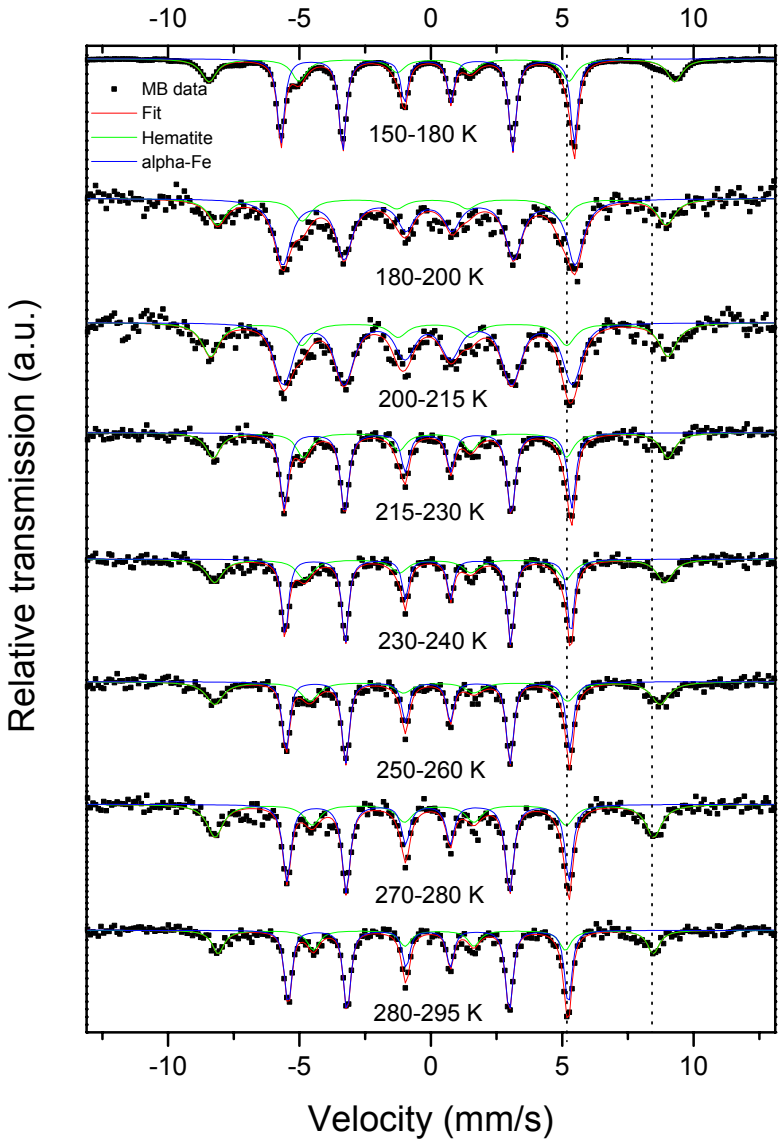

Figure 9b, Klingelhoefer et al. [2003]

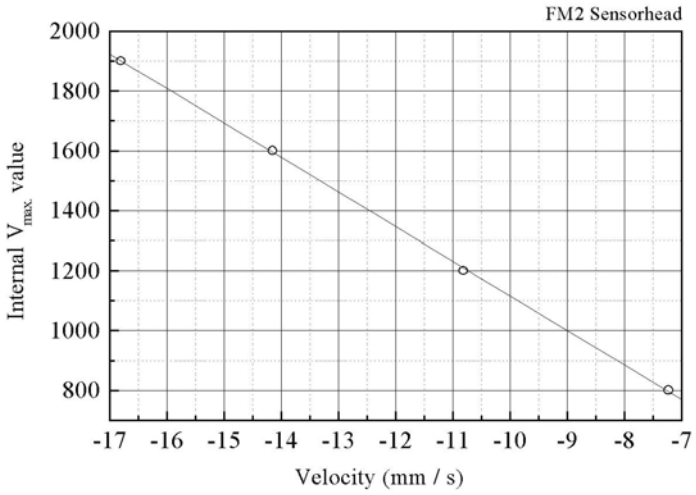

Figure 10, Klingelhoefer et al. [2003]

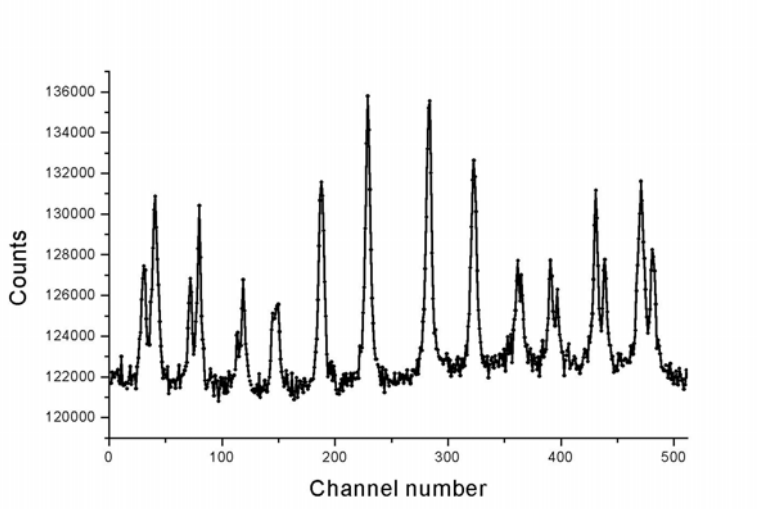

Figure 11, Klingelhoefer et al. [2003]

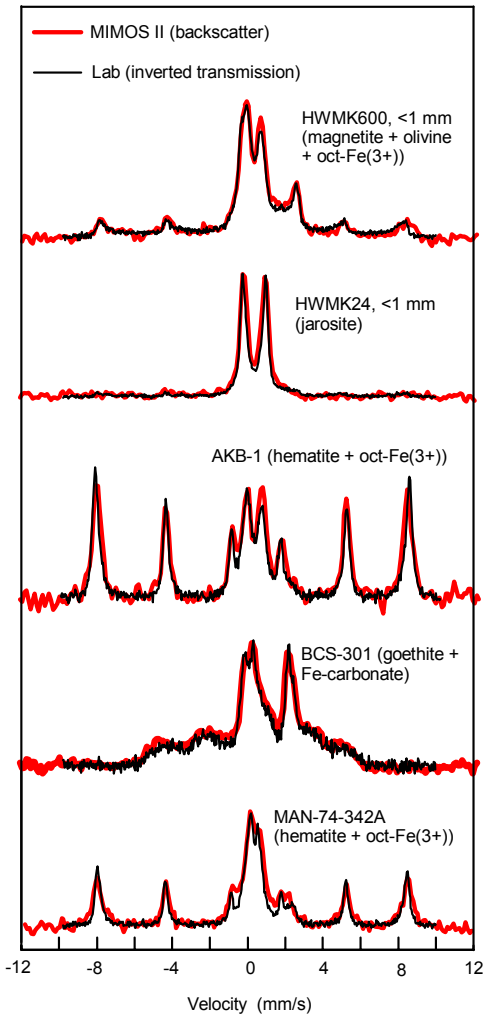

Figure 12, Klingelhoefer et al. [2003]

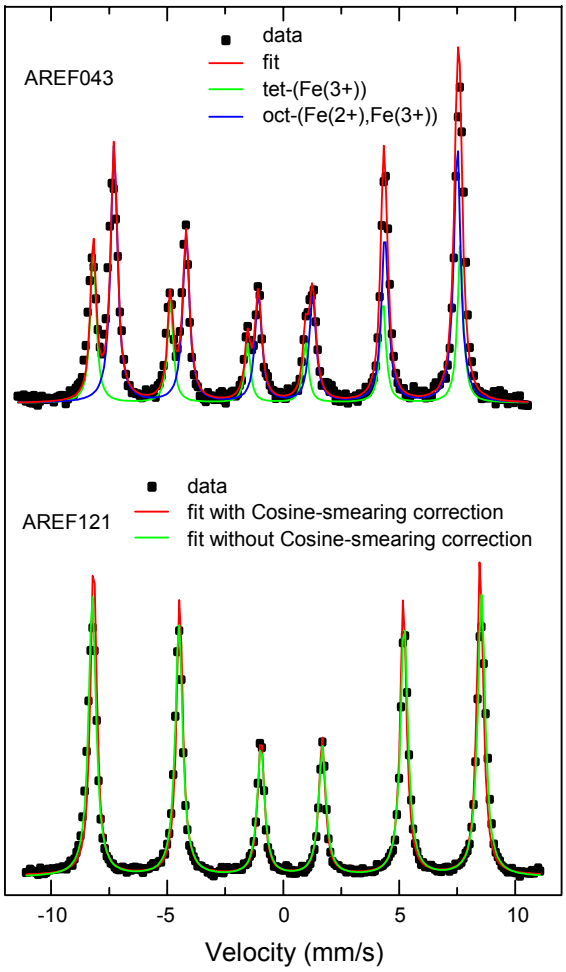

Figure 13, Klingelhoefer et al. [2003]

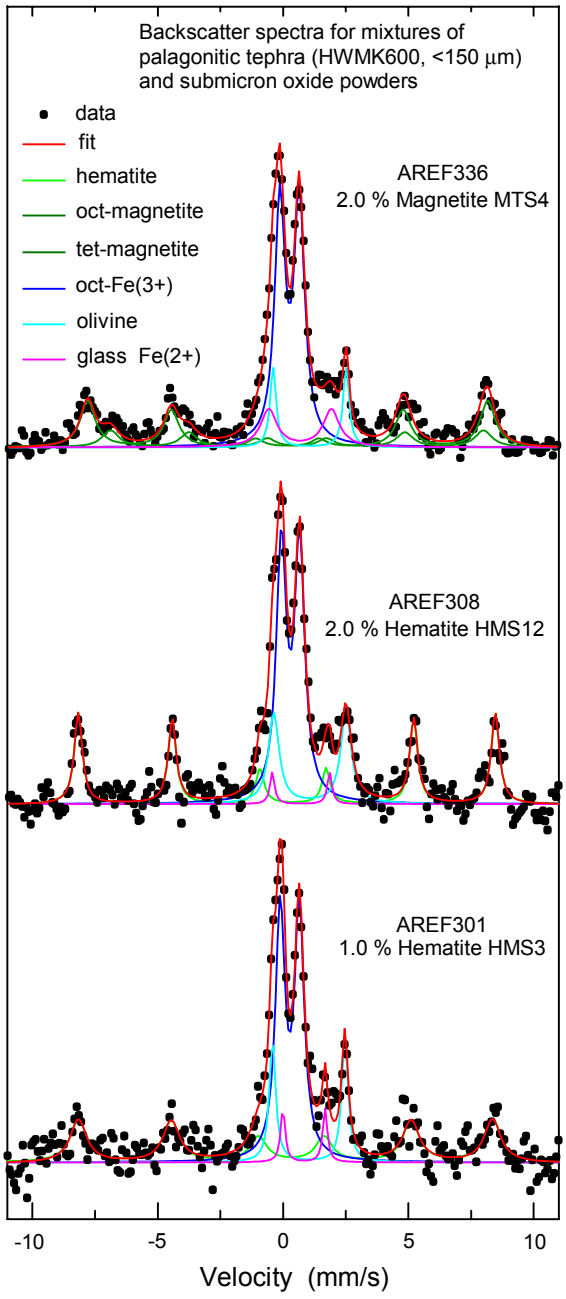

Figure 14, Klingelhoefer et al. [2003]